The Astrophysical Journal, 703:441–460, 2009 September 20 doi:10.1088/0004-637X/703/1/441

YELLOW SUPERGIANTS IN THE ANDROMEDA GALAXY (M31)*

Maria R. Drout[1,4], Philip Massey[1,5], Georges Meynet[2], Susan Tokarz[3], and Nelson Caldwell[3]
[1] Lowell Observatory, 1400 W Mars Hill Road, Flagstaff, AZ 86001, USA; maria-drout@uiowa.edu, Phil.Massey@lowell.edu
[2] Geneva University, Geneva Observatory, CH-1290 Versoix, Switzerland; georges.meynet@unige.ch
[3] Smithsonian Astrophysical Observatory, 60 Garden Street, Cambridge, MA 02138, USA; tokarz@cfa.harvard.edu, caldwell@cfa.harvard.edu
Received 2009 May 20; accepted 2009 August 4; published 2009 August 27

ABSTRACT

The yellow supergiant content of nearby galaxies can provide a critical test of stellar evolution theory, bridging the gap between the hot, massive stars and the cool red supergiants. But, this region of the color–magnitude diagram is dominated by foreground contamination, requiring membership to somehow be determined. Fortunately, the large negative systemic velocity of M31, coupled to its high rotation rate, provides the means for separating the contaminating foreground dwarfs from the bona fide yellow supergiants within M31. We obtained radial velocities of ∼2900 individual targets within the correct color–magnitude range corresponding to masses of 12 $M_{\odot}$ and higher. A comparison of these velocities to those expected from M31's rotation curve reveals 54 rank-1 (near certain) and 66 rank-2 (probable) yellow supergiant members, indicating a foreground contamination $\geqslant$ 96%. We expect some modest contamination from Milky Way halo giants among the remainder, particularly for the rank-2 candidates, and indeed follow-up spectroscopy of a small sample eliminates four rank 2's while confirming five others. We find excellent agreement between the location of yellow supergiants in the H-R diagram and that predicted by the latest Geneva evolutionary tracks that include rotation. However, the relative number of yellow supergiants seen as a function of mass varies from that predicted by the models by a factor of >10, in the sense that more high-mass yellow supergiants are predicted than those are actually observed. Comparing the total number (16) of $> 20\ M_{\odot}$ yellow supergiants with the estimated number (24,800) of unevolved O stars indicates that the duration of the yellow supergiant phase is ∼3000 years. This is consistent with what the 12 $M_{\odot}$ and 15 $M_{\odot}$ evolutionary tracks predict, but disagrees with the 20,000–80,000 year timescales predicted by the models for higher masses.

Key words: galaxies: individual (M31) – galaxies: stellar content – stars: evolution – supergiants

Online-only material: color figures, machine-readable table

1. INTRODUCTION

The color–magnitude diagrams (CMDs) of nearby galaxies reveal the details of stellar evolutionary processes, if our eyesight is keen enough. In recent years both the data and theory have made considerable advances. On the one hand, large format CCD cameras have allowed comprehensive photometry of the resolved stellar content of nearby galaxies, such as that of the Local Group Galaxy Survey (LGGS), which imaged those Local Group galaxies with active star formation (Massey et al. 2006, 2007a, 2007b). On the other hand, recent advances in stellar evolutionary theory have demonstrated the important role that rotation plays in the evolution of massive stars (see, for example, Maeder & Meynet 2000; Meynet & Maeder 2003, 2005).

Consider the optical CMD of the Andromeda Galaxy (M31), shown in Figure 1(upper). The unevolved stars are found on the left, in the section labeled "Blue Supergiants." However, this "blue plume" in such diagrams actually contain a mix of both unevolved main sequence and more evolved blue supergiants (Freedman 1988); it also contains a smattering of Wolf–Rayet stars (WRs), the evolved descendants of the most massive O-type stars. Massey et al. (1995) have emphasized that the optically brightest stars in this region of the CMD are not, in fact, the most bolometrically luminous or massive—rather, the brightest stars are dominated by B- and A-type supergiants, while more massive (and luminous) O-type stars are fainter as most of their radiation lies in the far-UV.

The central portion of the CMD contains the yellow supergiants, and at the extreme right, the red supergiants (RSGs). But, redwards of the blue plume caution is advised in our interpretation, as foreground contamination may dominate. We demonstrate this in Figure 1 lower by using the Besancon model (Robin et al. 2003) of the Milky Way to construct a theoretical CMD of the expected foreground contamination, using the same galactic coordinates as M31, and covering the same area. For the bright stars ($V < 20$) redwards of the blue plume ($B - V > 0.4$) the foreground contamination is > 70%. Note that the features in the M31 "yellow plume" area are well reproduced by the Besancon model. In Figure 2 we break down this foreground contamination into its various components. The disk populations clearly dominate, but even among the brighter stars there will be some contamination by halo giants and subgiants.

Our group is engaged in the long-term process of characterizing the massive star populations of nearby galaxies from one side of the CMD to the other. In order to relate this to evolutionary theory, we must succeed in two things: first, to be able to clean foreground stars from the sample, and second to provide a transformation of observed properties to physical properties. We have recently undertaken this for the RSGs of M31 (Massey et al. 2009); here we turn our attention to the yellow supergiants.

* Observations reported here were obtained at the MMT Observatory, a joint facility of the University of Arizona and the Smithsonian Institution.
[4] Research Experience for Undergraduates (REU) participant, Summer 2008. Present address: Department of Physics & Astronomy, University of Iowa, Iowa City, IA 52245.
[5] Visiting Astronomer, Kitt Peak National Observatory, National Optical Astronomy Observatory, which is operated by the Association of Universities for Research in Astronomy, Inc. (AURA) under cooperative agreement with the National Science Foundation.

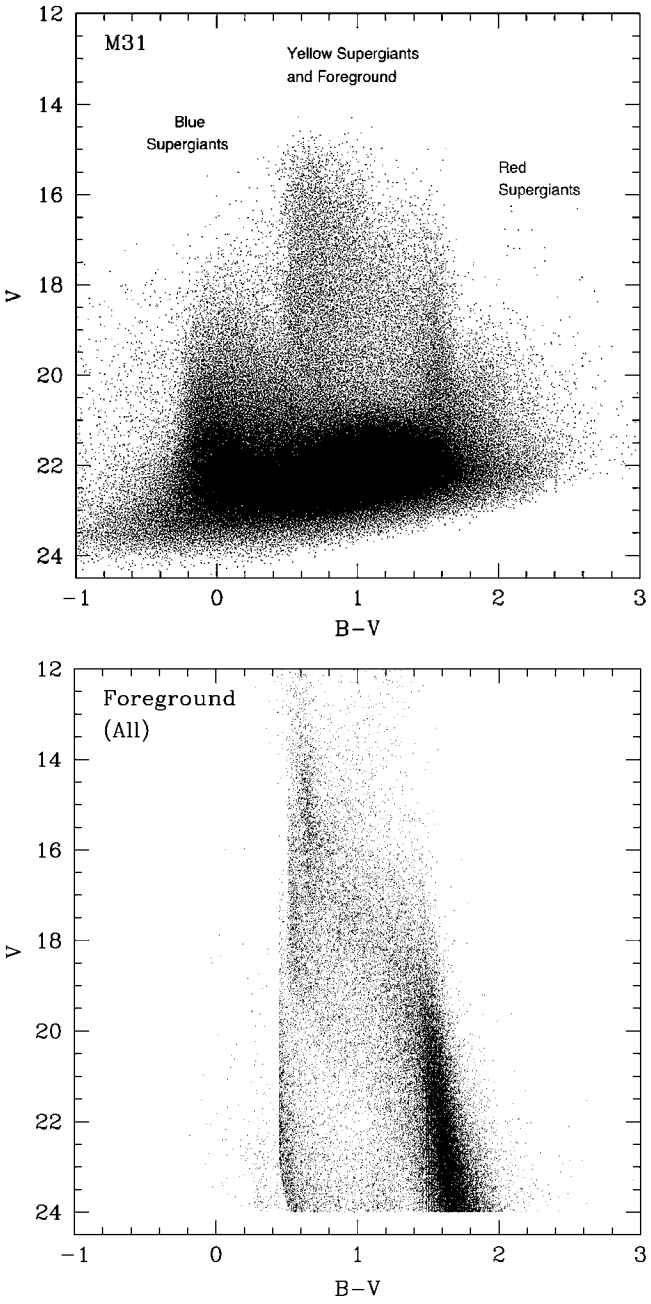

Figure 1. CMDs. Upper: the LGGS photometry is used to construct a CMD for M31. Lower: the regions of large foreground contamination in the M31 diagram can be inferred from a CMD constructed using the Besancon model (Robin et al. 2003) of the Milky Way.

1.1. Yellow Supergiants as a Magnifying Glass

Yellow supergiants (F- and G-type) are extremely rare, as they represent a very short-lived phase in the evolution of massive stars. Their numbers and location in the H-R diagram (HRD) are very sensitive to the uncertain values of the mass-loss rates for massive stars, and how convection and other mixing processes are treated (Maeder & Meynet 2000). As Kippenhahn & Weigert (1990, p. 468) put it, "[The yellow supergiant] phase is a sort of magnifying glass, revealing relentlessly the faults of calculations of earlier phases."

Exactly how sensitive our expectations should be to the details of the models is illustrated by comparing the various Geneva evolutionary models (Schaller et al. 1992; Charbonnel et al. 1993; Schaerer et al. 1993; Maeder & Meynet 2001; Meynet & Maeder 2003, 2005) shown in Figure 3 and the corresponding lifetimes for the yellow supergiant stage given in Table 1.[6] The metallicities shown span a range of 10, from sub-solar ($z = 0.004$, typical of the Small Magellanic Cloud (SMC)) to solar ($z = 0.020$) to super-solar ($z = 0.040$, typical of M31); see Massey (2003) and references therein. Solid curves denote the latest models computed with an assumed initial rotation of 300 km s^{-1},the dashed curves are the latest models that include no initial rotation, and the dotted curves are the older, nonrotating models. Since different versions (rotating, newer nonrotating, older nonrotating) of the same mass track differ in luminosity, we have color coded them for clarity; the corresponding initial mass is shown in the same color. The two solid vertical lines denote the yellow supergiant region, which we define as having effective temperatures between 4800 K and 7500 K.

We see that in most cases the models predict a short pass through the yellow supergiant region as stars evolve from the OB main-sequence stage (off the plot to the left) over to the RSG region on the right. However, in some cases, such as the evolutionary track that includes rotation (solid curve) for 25 $M_\odot$ at Galactic metallicity ($z = 0.020$) the star then evolves back to the blue side of the HRD. At higher masses (40–60 $M_\odot$) the models predict that a star will double back to the blue side during the yellow supergiant phase rather than passing through a red supergiant phase. The lifetimes for the yellow supergiant stage given in Table 1 are all very short, typically a few tens of thousands of years. The main-sequence lifetimes of these stars are a few million years, so, in general, the yellow supergiant lifetimes are on the order of 1% or less. In the extreme cases (lifetimes of the yellow supergiant phase of ∼3000 yr for a 12 $M_\odot$ star with 15 Myr lifetime) it is of order 0.02%. We do see from Table 1, however, exactly how sensitive these yellow supergiant lifetimes are to the exact treatments of the models. At Galactic metallicities, the models computed with an initial rotational speed of 300 km s^{-1} ("S3") indicate a 10× shorter yellow supergiant phase than models with the same assumptions but with no initial rotation ("S0").

There are also clearly differences in the expected *locations* of the yellow supergiants in the HRD, particularly those of the highest luminosities. According to the models, for instance, at $\log L/L_\odot \sim 5.8$ dex we would expect to see some yellow supergiants at Galactic ($z = 0.020$) metallicities, but only the hotter ones (i.e., $T_{\rm eff} > 6000$ K), while at lower luminosities we should find stars populating throughout the region. The duration of the yellow supergiant phase is not significantly shorter for a higher mass (luminosity) star than for a lower mass (luminosity) star, according to Table 1—if anything the opposite is true—so simply determining the upper luminosity limit to yellow supergiants at various metallicities would be of great interest for comparison with the models, as well as seeing if the number of higher mass yellow supergiants really comparable to that of lower masses.

We emphasize that such a test is new, and avoids some of the selection biases that may dominate comparisons of one population of massive stars to another, such as comparing the number of yellow and RSGs, or the number of RSGs and WRs. Although those tests are invaluable, they require a thorough

[6] Note that the 20 $M_\odot$ and 25 $M_\odot$ $z = 0.040$ models of Meynet & Maeder (2005) were computed using a numerical simplification which resulted in the tracks turning back to the blue at too high an effective temperature; here we use the recomputed versions mentioned in Massey et al. (2009). We also include here newly completed $z = 0.040$ models for 12 $M_\odot$ and 15 $M_\odot$ which include the effects of rotation.

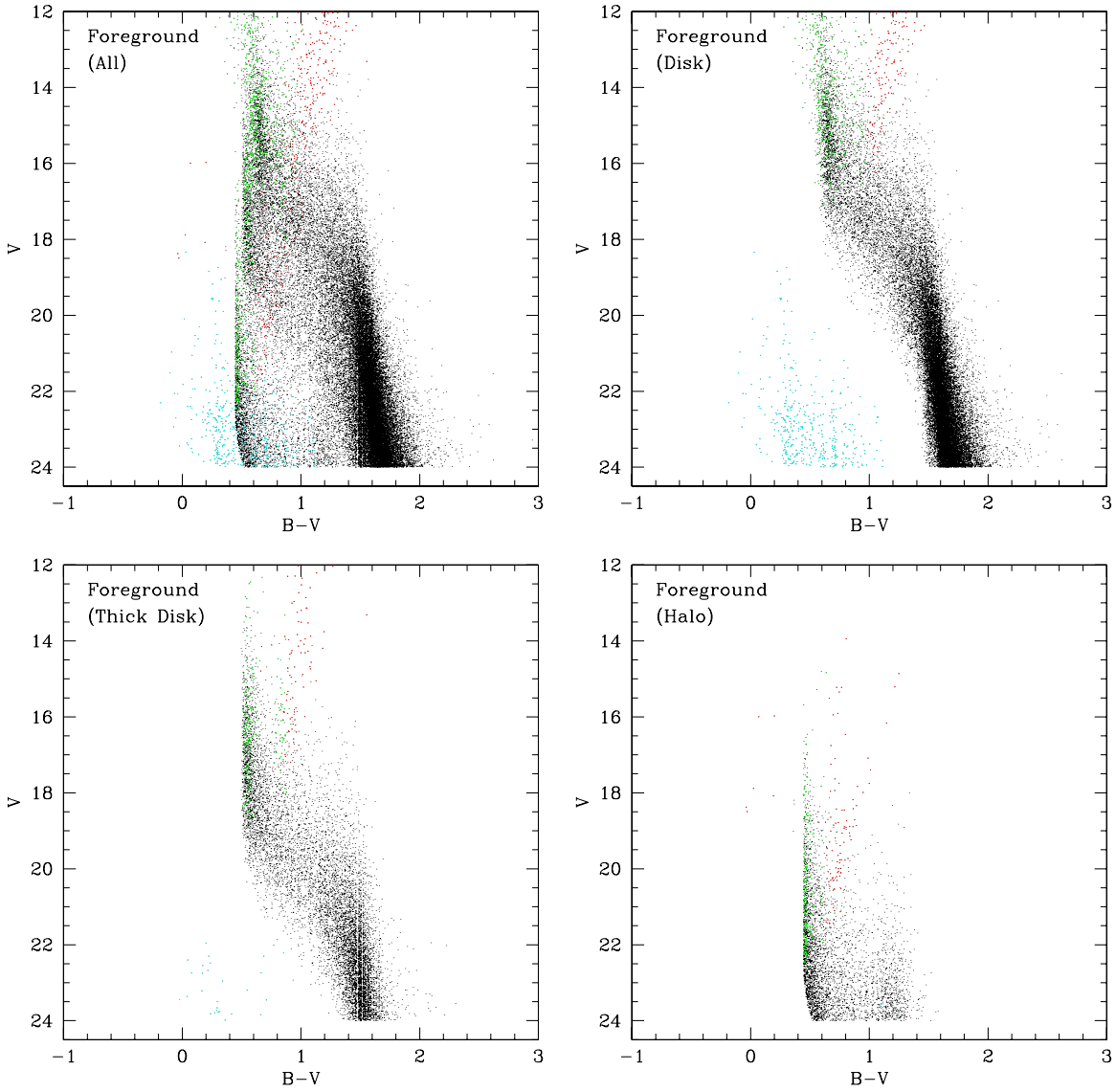

Figure 2. Components of the foreground contamination of the M31 field identified using the Besancon model. In the upper left, we show the expected foreground contamination of the M31 field, where we have color coded the giants (red), subgiants (green), and the white dwarfs (cyan). The remaining points are primarily main-sequence dwarfs. In the other three panels, we further break down the distribution into the disk component (upper right), the thick disk component (lower left), and the halo component (lower right).

(A color version of this figure is available in the online journal.)

understanding of the completeness of the surveys of such objects. We make progress toward gathering the information that make such further tests possible (see summary given in Massey 2009).

1.2. Separating the Wheat from the Chaff

We have previously found that it is straightforward to separate (extragalactic) RSGs from (foreground) red dwarfs and giants by using a two-color diagram (Massey 1998a, Massey et al. 2009), but this discrimination does not extend to the yellow supergiants. In Figure 4(upper), we show the intrinsic color lines from FitzGerald (1970). The dwarf sequence is shown in green, and the supergiant sequence in red. We have reddened the supergiant sequence slightly, by $E(B-V) = 0.13$, corresponding to the typical reddening of a massive star in M31 (Massey et al. 2007b); this slight adjustment down and to the right is shown by the short bar in lower left. Superimposed on this two-color diagram are the stars brighter than $V = 18.5$ from the LGGS photometry given by Massey et al. (2006) for stars in M31.

For the mid-F-type stars, there is a separation in the sense that for a given $B-V$ a supergiant will have a larger $U-B$. For early-A-type supergiants this trend is reversed; i.e., supergiants will have a more negative $U-B$. However, as is clear from this plot there is little or no separation in the two-color diagram for supergiants of late A or early F, or for supergiants of late F through early K. Examination of other colors (using model atmospheres) failed to identify any more suitable diagnostic two-color tool.

It is also clear from distribution of points in this figure that the majority of blue stars are expected to be supergiants, while the majority of stars of later types may well be foreground, as we argued above. We illustrate this further in Figure 4 (lower), where we have used the Besancon simulation of the Milky Way (Robin et al. 2003) to show the expected distribution of

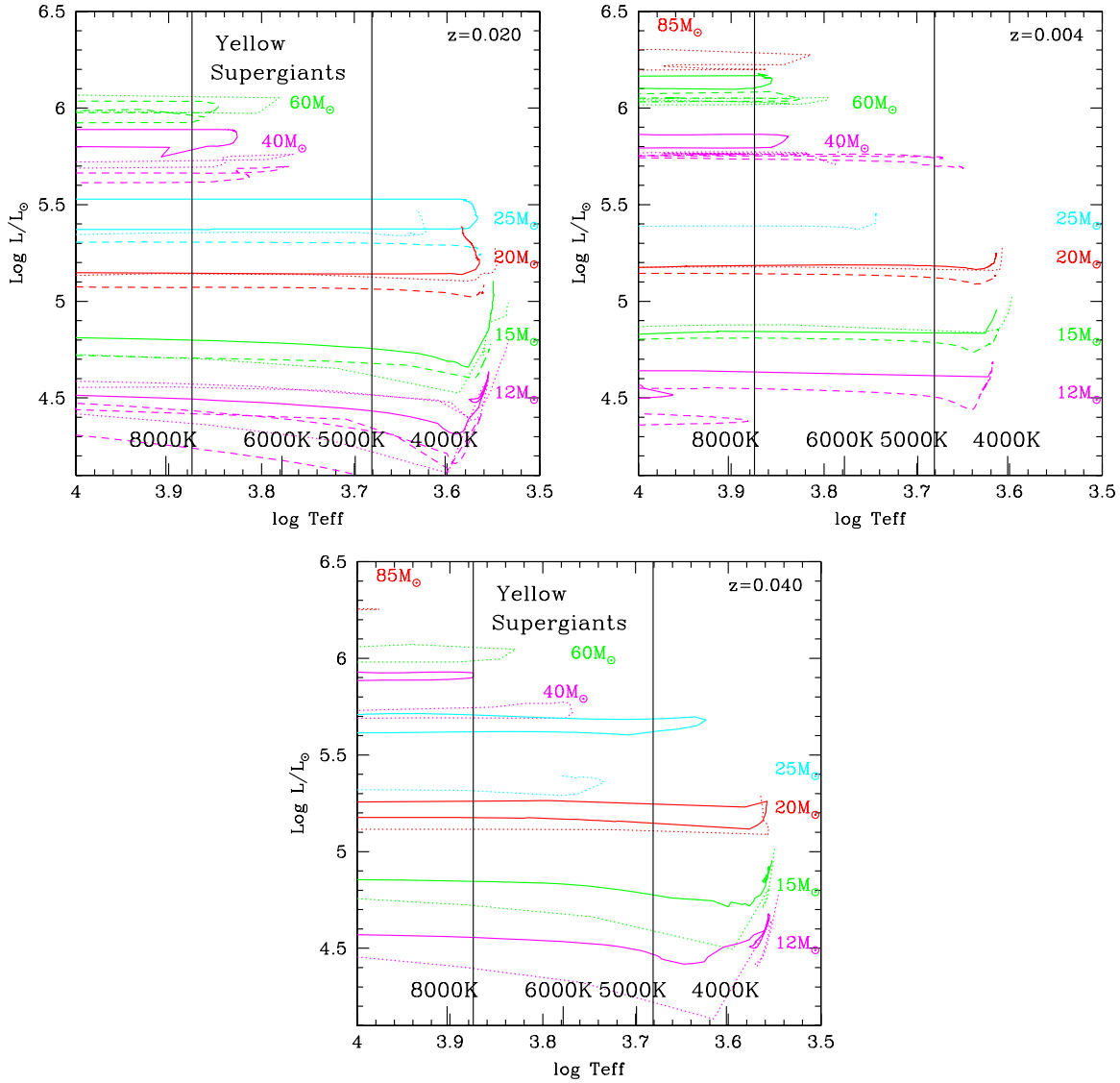

Figure 3. Geneva evolutionary tracks. The solid curves denote the latest models that include an initial rotation of 300 km s^{-1}, the dashed curves are the latest models that include no initial rotation, and the dotted curves are the older, nonrotating models. The various versions of the tracks appear in the same color for a given mass to reduce the confusion. The two vertical lines denote the yellow supergiant region, taken to be when the models have 4800 K $\leqslant T_{\rm eff} \leqslant$ 7500 K. The tracks are shown for three metallicities: $z = 0.020$ is characteristic of the solar neighborhood, $z = 0.004$ is characteristic of the SMC, and $z = 0.040$ is characteristic of M31.

(A color version of this figure is available in the online journal.)

foreground stars in such a diagram. The comparison between the two sides of the figures reveals where we expect foreground stars to dominate.

Given the lack of two-color discriminants, what then are our options to identify a relatively complete sample of yellow supergiants that can be used to test the stellar evolution models? Uncertain distances and reddening complicate the analysis of a galactic sample. In her compilation of 949 supergiants known in the Milky Way, Humphreys (1978) lists just 21 supergiants of spectral type F0-G9 I (i.e., about 2%). Even so, several of these have dubious cluster memberships and, hence, uncertain luminosities. In the Magellanic Clouds there are less than a dozen spectroscopically confirmed F and G supergiants (Oestreicher & Schmidt-Kaler 1999), although this deficiency may be largely due to the lack of adequate spectroscopic studies in the correct magnitude/color range, a situation we ourselves hope to remedy in the not too distant future.

We have concluded that M31 provides the best laboratory for conducting such tests at present, as its kinematics allow us to overcome the problems posed by foreground contamination of its CMD. M31 possesses a large negative systemic velocity (~ -300 km s^{-1}) and a high rotation rate (240 km s^{-1}), making it relatively straightforward to demonstrate membership based on radial velocities. Gilbert et al. (2006) and Koch et al. (2008) similarly used radial velocities to separate M31's red giant members from foreground contamination. The recent LGGS photometry of M31 (Massey et al. 2006) provides the means for selecting candidate stars for radial velocities, and for transforming intrinsic colors to physical properties.

In this paper we conduct a census of yellow supergiants in M31, establishing membership, determining physical properties, and making comparisons with the current generation of evolutionary tracks. In Section 2, we describe our data and reduction. In Section 3, we illustrate the process by which we separated foreground dwarfs from M31's yellow supergiants, and in Section 4 we present the comparison of our results to the current evolutionary tracks. We provide discussion and lay out our thoughts for future work in Section 5.

Table 1
Theoretical Yellow Supergiant Duration (yr)[a]

Mass	Solar Neighbor $z = 0.020$			SMC $z = 0.004$			M31 $z = 0.040$		
($M_\odot$)	S3[b]	S0[b]	Old[c]	S3[d]	S0[e]	Old[f]	S3[d]	S0[d]	Old[g]
85	0	0	0	...	...	12300	0	...	0
60	0	14100	5300	14000	56500	62300	0	0	5400
40	57600	403600	198100	148100	32700	188200	50800	...	87300
25	5400	73000	23600	...	...	109800	18500	...	666000
20	300	92500	64800	71700	16500	58900	78300	...	3800
15	2100	50800	2300	206600	60400	92000	3200	...	1900
12	3600	32800	51000	33200	30700	21800	5300	...	2500

Notes.
[a] For the purposes of this calculation, yellow supergiants are defined as having effective temperatures between 4800 K and 7500 K. Note that not all versions of the evolutionary models are available for each mass and metallicity.
[b] S3 has initial rotation 300 km s^{-1}, and S0 has an initial rotation of 0 km s^{-1}; ages were determined using models from Meynet & Maeder (2003).
[c] Rotation not included; determined using models from Schaller et al. (1992).
[d] S3 has an initial rotation of 300 km s^{-1}, and S0 has an initial rotation of 0 km s^{-1}; ages were determined using models from Meynet & Maeder (2005), except for the 9, 12, 20, and 25 $M_\odot$, $z = 0.040$ models newly computed for this study and that of Massey et al. (2009), and the 12, 15, and 20 $M_\odot$, $z = 0.004$ models from Maeder & Meynet (2001).
[e] The S0 models for $z = 0.004$ were computed with an initial rotation of 0 km s^{-1}; ages were determined using the models from Maeder & Meynet (2001).
[f] Rotation not included; determined using models from Charbonnel et al. (1993).
[g] Rotation not included; determined using models from Schaerer et al. (1993).

2. OBSERVATIONS AND REDUCTIONS

In order to separate yellow foreground dwarfs from the yellow supergiants, we used the Hectospec fiber spectrograph on the 6.5 m MMT telescope to obtain radial velocities for $\sim$ 2900 stars. In this section we describe the sample selection, data acquisition, and reductions.

2.1. Sample Selection

Our sample of objects was selected to have $V < 18.5$ (roughly corresponding to $\log L/L_\odot \sim 4.4$) to provide adequate signal-to-noise for our spectroscopy. The color range was originally restricted to $U - B > -0.4$ with $0.4 \leqslant B - V \leqslant 1.4$ in accordance with the range of $B-V$ for which dwarfs and supergiants cannot be distinguished photometrically; however, we found that relaxing the color range to $0.0 \leqslant B - V \leqslant 1.4$ added only a small percentage of additional stars.

Our other selection criteria were based upon the need to be able to distinguish the M31 yellow supergiants from foreground disk dwarfs based upon their radial velocities. Inspection of the atlas of Galactic neutral hydrogen by Hartmann & Burton (1997) shows that M31 (at $l = 121.^\circ2$, $b = -21.^\circ6$) clearly stands out from the Galactic clutter at a radial velocity of -150 km s^{-1} (see Hartmann & Burton 1997, p. 87), but is somewhat confused by -100 km s^{-1} (pp. 95, 97). We therefore decided to restrict our observations to those areas in M31 where the radial velocities should be $\leqslant -150$ km $^{-1}$. For computing the expected radial velocity corresponding to a position in M31, we used Rubin & Ford (1970), the seminal paper on the rotation of M31. A least-squares linear fit to the radial velocities of the H II regions yields the expected radial velocities $\mathrm{Vel}_{\mathrm{expect}}$

$$\mathrm{Vel}_{\mathrm{expect}} = -295 + 241.5(X/R),$$

where X is the distance along the semimajor axis, and R is the radial distance of the object within the plane of M31. We found that this approximation works well, producing good agreement with the more complex two dimension velocity field (Sofue & Kato 1981), and with other recent approximations (Hurley-Keller et al. 2004). The radial velocities of RSGs in M31 also agree well with this simple relationship (Massey et al. 2009).

The result of this selection criterion is that not all of the area surveyed in the LGGS was included in our sample: stars along the southwest half of the semimajor axis of M31 ($X/R \sim -1$) will have radial velocities of ~ -550 km s^{-1}, but stars along the northeast half of the semimajor axis ($X/R \sim 1$) will have radial velocities of -50 km s^{-1}, more positive than our selection criterion of -150 km s^{-1}. The distribution of stars in our sample is shown in Figure 5, where the "jaws" in the northeast (upper left) are due to stars near the semimajor axis having smaller R values than those seen along the edge of the disk. In all our sample covered 1.6 deg^2 of the 2.2 deg^2 of the LGGS survey (i.e., about 73%).

We were concerned that a few legitimate F or G supergiants *might* be too bright to be included in the LGGS photometry, particularly due to saturation in the R filter around $R \sim 15.5$. We therefore supplemented the LGGS data with 163 bright ($V < 16.0$) stars from the survey of Magnier et al. (1992). In order to prevent mixing bright and faint stars in the same observations, we then divided our overall catalogs into a "bright" catalog (349 stars with $V < 16.0$) and a "faint" catalog (3994 stars with $15.5 < V < 18.5$), with 61 objects in common. Due to the constraints of the fiber configurations, not all the objects could be observed, but we did manage to observe 68% of the 4282 catalog targets.

2.2. Spectroscopy

Hectospec is a 300 optical fiber fed spectrograph (Fabricant et al. 2005) on the MMT 6.5 m telescope. Observations are obtained in an innovative queue mode where the observers are the astronomers who were awarded time, but with the observing

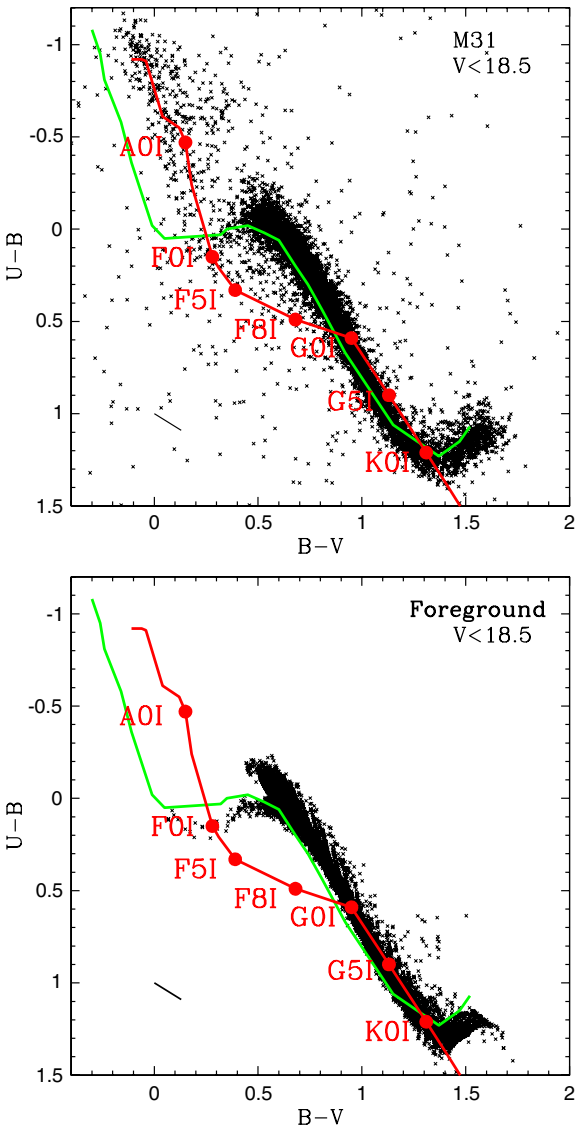

Figure 4. Two-color diagram. The intrinsic two-color relationships are shown for dwarfs (green) and supergiants (red), from FitzGerald (1970). Upper: the points show the photometry from the LGGS of M31 (Massey et al. 2006). The supergiant sequence has been reddened for a typical $E(B-V) = 0.13$, with the reddening vector shown by the short line in the lower left. Lower: the points show the approximate foreground contamination from the Milky Way for the same solid angle and Galactic latitude and longitude as the M31 photometry. The data come from a simulation with the Besancon model (Robin et al. 2003).

(A color version of this figure is available in the online journal.)

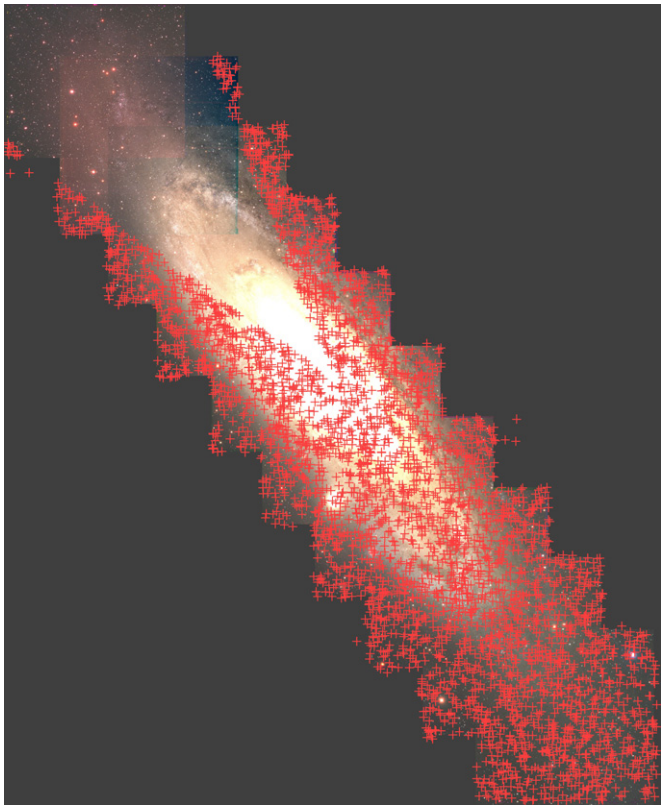

Figure 5. Distribution of our sample across the face of M31. The M31 image is a mosaic of the 10 LGGS $36' \times 36'$ fields. The stars selected for our sample are shown by the red points. The requirement that the expected rotational velocity be $\leqslant -150$ km s^{-1} results in the "alligator jaw" pattern. The figure is slightly smaller than the area over which the LGGS has photometry, and hence a few points fall outside the image of the galaxy.

(A color version of this figure is available in the online journal.)

program for a given night determined by a queue manager. The observers are ably assisted by one of the two professional instrument operators, in addition to the telescope operator. This "collective" approach spreads out the effects of poor weather throughout the observing season, reducing the impact on any one program. Our observations were all carried out on eight nights during 2007 October and one night in 2007 November. The 600 line mm^{-1} grating was used, providing a dispersion of 0.55 Å pixel^{-1} and a (5 pixel) spectral resolution of 2.8 Å. The wavelength coverage extended from 4550 to 7050 Å.

The fiber configuration files were constructed prior to the observations. The instrument has a 1° field of view, a reasonable match to the 3°–4° angular extent of the optical disk of M31 (Hodge 1981). Our observations consisted of observing a single configuration for each of the five fields containing the brighter stars ("Brt" fields), and multiple configurations of three fields containing the fainter stars ("Fnt" fields), as listed in Table 2. Observations of each "Brt" configuration consisted of three consecutive exposures of 10 minutes each, while observations of the "Fnt" configurations consisted of three consecutive exposures of 15 minutes each. In the end, we obtained 3116 spectra of 2901 of our catalog targets.

Owing to the logistics of the queue observations, calibration exposures (flat field and He–Ne–Ar) were taken only in the afternoon, and subsequent to that the grating might have been tilted to a different angle to accommodate other programs, or even removed entirely and then replaced for our observations. We deal with this complication as described below.

We also needed observations of stars that could serve as templates for the cross-correlation. Since the 600 line mm^{-1} is not commonly used, we obtained our own observations of three radial velocity standards, HD 196850, HD 194071, and HD 213014. HD 213014 was observed on four different nights.

2.3. Data Reduction

The data were all reduced using the "hectospec" IRAF[7] package, designed specifically for this instrument (Mink et al. 2007). The data were bias-subtracted, trimmed, and a bad pixel extrapolation was performed using pre-existing bad pixel

[7] IRAF is distributed by NOAO, which is operated by AURA under cooperative agreement with the NSF. We appreciate the on-going support of IRAF by the volunteers at the IRAF help "desk," http://www.iraf.net.

Table 2
Configurations Observed

Configuration	α_{2000}	δ_{2000}	Exps	UT Date(s)	*N* stars observed
Brt1-1	00 46 49.0	+42 11 21	3 × 10 min	2007 Oct 23	15
Brt2-1	00 44 00.8	+41 37 28	3 × 10 min	2007 Oct 14	92
Brt3-1	00 41 39.6	+40 51 30	3 × 10 min	2007 Oct 14	93
Brt4-1	00 40 46.9	+40 36 36	3 × 10 min	2007 Oct 16	111
Brt5-1	00 39 32.4	+40 21 33	3 × 10 min	2007 Oct 17, 2007 Oct 23	128
Fnt1-1	00 38 55.8	+40 07 38	3 × 15 min	2007 Oct 14	201
Fnt1-2	00 39 09.8	+40 09 24	3 × 15 min	2007 Oct 14	202
Fnt1-3	00 38 48.1	+40 06 49	3 × 15 min	2007 Oct 16	191
Fnt1-4	00 38 56.0	+40 07 37	3 × 15 min	2007 Oct 16	170
Fnt1-5	00 39 06.3	+40 06 54	3 × 15 min	2007 Oct 17	148
Fnt1-6	00 39 09.0	+40 07 06	3 × 15 min	2007 Oct 18	109
Fnt2-1	00 41 48.9	+40 55 23	3 × 15 min	2007 Oct 19	199
Fnt2-2	00 41 37.9	+40 54 30	3 × 15 min	2007 Oct 19	198
Fnt2-3	00 41 26.7	+40 54 49	3 × 15 min	2007 Oct 20	200
Fnt2-4	00 41 26.8	+40 54 13	3 × 15 min	2007 Oct 20	191
Fnt2-5	00 41 38.0	+40 54 30	3 × 15 min	2007 Oct 21	150
Fnt2-6	00 41 50.8	+40 55 17	3 × 15 min	2007 Oct 21	137
Fnt3-1	00 44 05.6	+41 34 16	3 × 15 min	2007 Nov 20	151
Fnt3-2	00 44 29.3	+41 38 49	3 × 15 min	2007 Nov 20	150
Fnt3-3	00 44 36.2	+41 43 33	3 × 15 min	2007 Nov 20	151

maps. The flat-field exposures were extracted for each fiber and normalized in order to make the pixel-to-pixel corrections. The He–Ne–Ar arc exposures were then extracted, and used to make a dispersion solution. A sixth order Chebyshev function was used for this, resulting in typically 0.04 Å residuals.

The program exposures were extracted, using the dome flat field exposures as reference, and wavelength corrected. As the He–Ne–Ar exposures were obtained in the afternoon, and the grating might even be removed and reinserted before the program exposures, a zero-point shift in wavelength was determined for each of the M31 spectra using the O I λ5577 night sky line. (As explained below, no such correction could be made for the very short exposures of the radial velocity standards.) Consecutive exposures of each M31 configuration were then summed, after cosmic rays were first identified and removed by comparing a median of the exposures to the individual exposures.

For sky subtraction, each fiber had to first be corrected for its own wavelength-dependent throughput, using either the dome flat exposures, or, preferably, twilight exposures, if the latter had been obtained. Each M31 configuration contained both preselected "clean" sky positions plus random locations that might prove clean enough to be used as a measure of the sky. For each program spectrum six of these sky spectra were selected. These were taken from positions nearby on the array in order to reduce any scattered light component. These skies were then used to construct an average sky for subtraction using the Singular Value Decomposition method (Mink & Kurtz 2001). No sky subtraction was needed for the bright radial velocity standards.

3. ANALYSIS

3.1. Observed Radial Velocities

The radial velocities of our 2901 program objects were obtained through a cross-correlation with suitable radial velocity standards. All cross-correlations were performed in the IRAF package "fxcor," which computes radial velocities via Fourier cross-correlation using a Gaussian to find the center and width of the calibration peak, following the method of Tonry & Davis (1979). Before the cross-correlations were computed, each individual spectrum had its continuum removed by first normalizing and then subtracting 1.0. The normalization was done interactively, using a 12th order cubic spline fit to the continuum. The cross-correlations were restricted to the range 4750–5550 Å and 5600–6800 Å in order to avoid the strongest night-sky emission.

As mentioned above, although the [O I] λ5577 emission line was adequate to correct the program spectra for the wavelength zero point (necessitated by the logistics of the queue) there was, ironically, no equivalent way to correct the radial velocity "standards." In order to resolve this issue, we used two velocity templates, created for a related project, generated from 270 line mm^{-1} Hectospec observations (Caldwell et al. 2009). The templates were created by first deriving an initial velocity from library templates (typically a K giant star) for spectra selected from a catalog of M31 star clusters. The spectra were shifted to zero velocity and sorted into crude spectral bins (F- and K-type) at which point the best spectra from each type were then combined to make new templates and the whole process was repeated. When we cross-correlated our "rv-standards" with these templates, the velocities produced by the two templates varied by $\leqslant$ 1.1 km s^{-1} for all six observations. A third template, based upon early-type spectra (A-type) gave a velocity $\sim$5 km s^{-1} more positive, and we chose not to use it.[8]

In order to obtain suitable velocities for the radial velocity standards the relative velocities of the standards to the templates were obtained via cross-correlation and corrected to heliocentric velocities. We were very pleased to find this process yielded velocities that agreed with the IAU adopted velocities to better than 5 km s^{-1}. This indicates that if we had simply adopted the standard velocities, with *no* corrections, the resulting error would not have been large enough to affect our results.

[8] We did find that the low-resolution templates produced problems when measured directly against our M31 observations obtained at higher dispersion, giving inconsistent results on the one field repeated on two nights. The differences were strongly correlated with velocities, which we interpreted as being due to cross-correlating two spectra of very different dispersions and velocities.

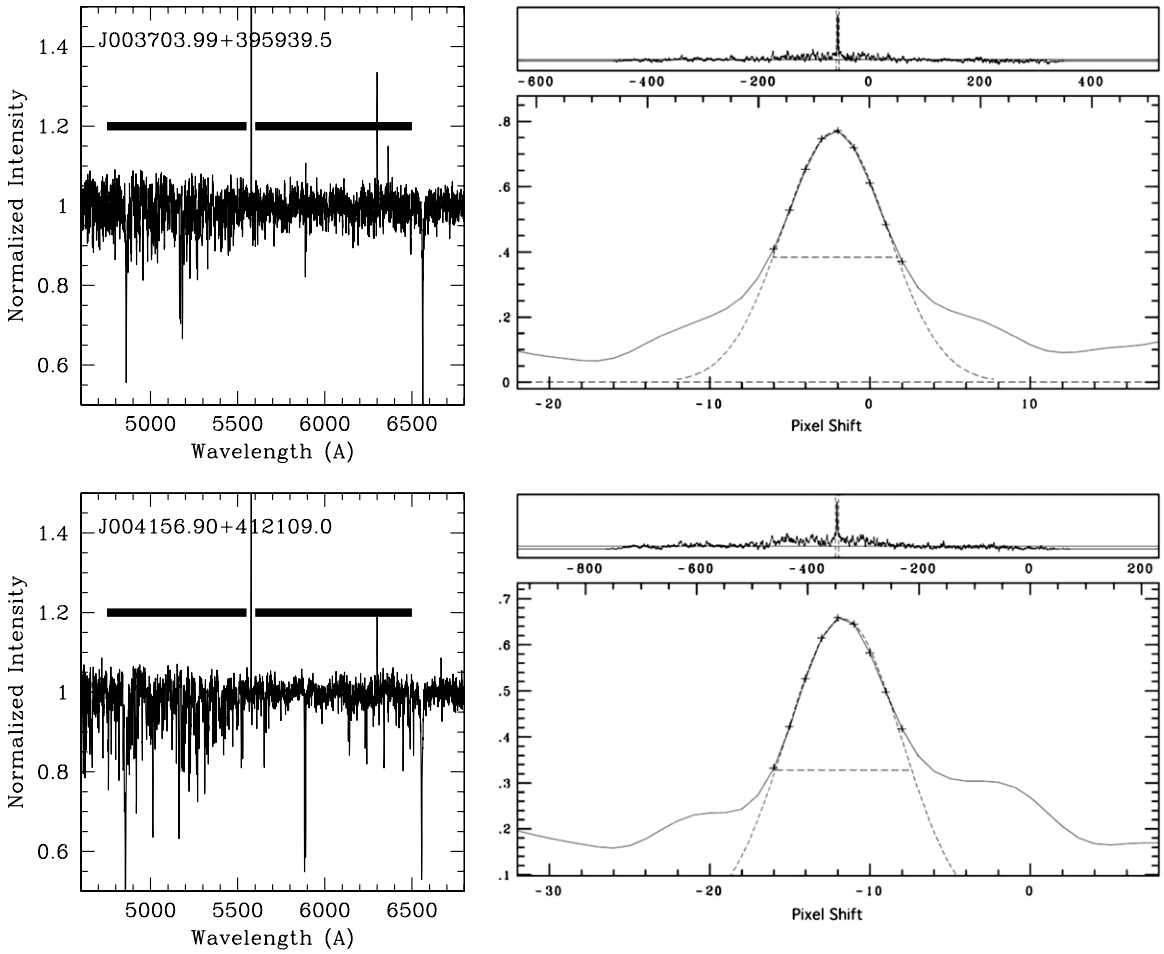

Figure 6. Examples of spectra and cross-correlations. We show sample spectra and the corresponding cross-correlation functions and fits. The thick bar shown on the spectra indicates the 4750–5550 Å, 5600–6500 Å regions used for the cross-correlation. The upper star, J00303.99+395939.5, proves to be a foreground dwarf (Section 3.2), with an average radial velocity of −48 km s^{-1} compared to −534 km s^{-1} expected for its position. The lower star, J004156.90+412109.0, proves to be an M31 supergiant (Section 3.2), with an average radial velocity of −335 km s^{-1} compared to −303 km s^{-1} expected for its position. Additional spectroscopy, discussed in Section 3.4, confirms that the star has very strong OI λ7774, a characteristic of a yellow supergiant.

As a final check of our newly adopted velocities, the standards were cross-correlated against each other. HD194071 and the four observations of HD213014 all produced velocities within 0.2 km s^{-1} of the standard value, and within 0.1 km s^{-1} of each other. HD196850, however, consistently produced velocities 0.5 km s^{-1} more positive. Although this value is not significant compared to the expected radial velocity difference between M31 yellow supergiants and galactic yellow dwarfs, it still prompted us to reject our spectrum of HD196850 as a radial velocity standard template. We then performed cross correlations of the five spectra of the radial velocity standards against each of the 3116 spectra of the 2901 program objects.

There were four objects for which our cross-correlations initially failed: J004101.24+410434.6; J004129.31+40502.9; J004203.63+405705.8; and J004459.11+412732.7. The spectra of all four objects were examined and strong nebular emission in the region of Hα was evident. When this region was excluded good correlations were found for J004101.24+410434.6 and J004129.31+40502.9, although their associated error was about twice as large as the average value of the other program objects.

We show in Figure 6 examples of two of our spectra, and their resulting cross-correlation functions and corresponding fits. These were selected to have V magnitudes typical of the median value in our entire sample, 17.1.

We list in Table 3 the observed radial velocity of each of our 2889 objects, some of which had multiple observations. What are the corresponding errors? Each observed radial velocity $\mathrm{Vel_{obs}}$ is the average of cross-correlating the star's spectrum against that of the five radial velocity standard spectra. The standard deviation of the mean of these is always very small, of order a few tenths of a km s^{-1}. However, the signal-to-noise in the standard templates is extremely high, and the standards are of similar type, so the differences in the velocities obtained from cross-correlating the same spectrum against these different standard spectra will certainly underestimate the true uncertanty. Tonry & Davis (1979) instead introduce the r parameter, which is the ratio of the peak of the correlation function to its noise. We can estimate the relationship between r and the error by using measurements obtained for stars observed multiple times. The 128 objects in the Brt5-1 field were observed on two separate nights, and in addition, there were 28 objects in common between the "bright" and "faint" fields, plus 59 objects observed in multiple "faint" fields. We find that in general our velocity error (in km s^{-1}) is given by

$$\mathrm{Vel_{err}} = 2.3 + 11.5/(1 + r),$$

Table 3
Stars with Observed Radial Velocities

Star	α_{2000}	δ_{2000}	Vel_{obs} (km s^{-1})	r[a]	Vel_{expect} (km s^{-1})	$Vel_{obs}-Vel_{exp}$ (km s^{-1})	V	$B-V$	Rank[b]
J003702.13+400945.6	00:37:02.127	+40:09:45.53	14.8	19.8	−513.5	528.3	16.09	1.29	3
J003702.47+401742.5	00:37:02.467	+40:17:42.42	−26.4	21.3	−487.7	461.3	18.03	1.32	3
J003702.80+400516.8	00:37:02.797	+40:05:16.74	−4.5	32.1	−524.9	520.4	16.79	0.71	3
J003702.94+400027.2	00:37:02.937	+40:00:27.14	−122.8	32.6	−532.8	410.0	17.96	0.84	3
J003703.78+395541.6	00:37:03.777	+39:55:41.55	−42.0	41.4	−536.3	494.3	15.76	0.74	3
J003703.85+401402.8	00:37:03.847	+40:14:02.73	−34.1	25.1	−501.2	467.1	17.38	1.22	3
J003703.99+395939.5	00:37:03.987	+39:59:39.44	−47.9	30.7	−533.9	486.0	17.08	0.69	3
J003704.12+401702.0	00:37:04.117	+40:17:01.93	−6.6	24.3	−491.1	484.5	15.91	0.97	3
J003704.53+401426.0	00:37:04.527	+40:14:25.93	−48.7	19.6	−500.4	451.7	17.88	0.60	3
J003704.56+400521.0	00:37:04.557	+40:05:20.94	−50.5	36.0	−525.5	475.0	17.83	0.77	3

Notes.
[a] Tonry & Davis (1979) r parameter.
[b] Rank: 1, highly likely supergiant; 2, probable supergiant; 3, dwarf; Cl, cluster.
[c] Radial velocity observed on two different nights differed by 10 km s^{-1} or more.

(This table is available in its entirety in a machine-readable form in the online journal. A portion is shown here for guidance regarding its form and content.)

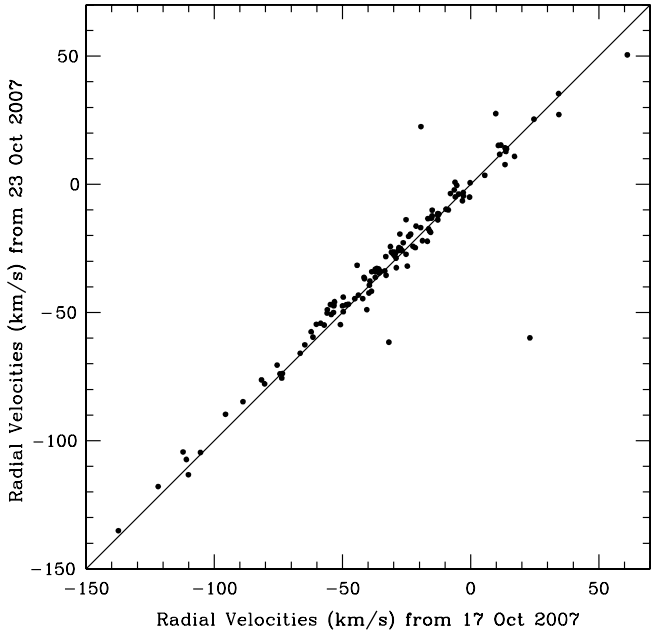

Figure 7. Radial velocity constancy. We show here a comparison of the observed radial velocities for the two observations of the Brt5-1 field. The line shows the 1:1 relation.

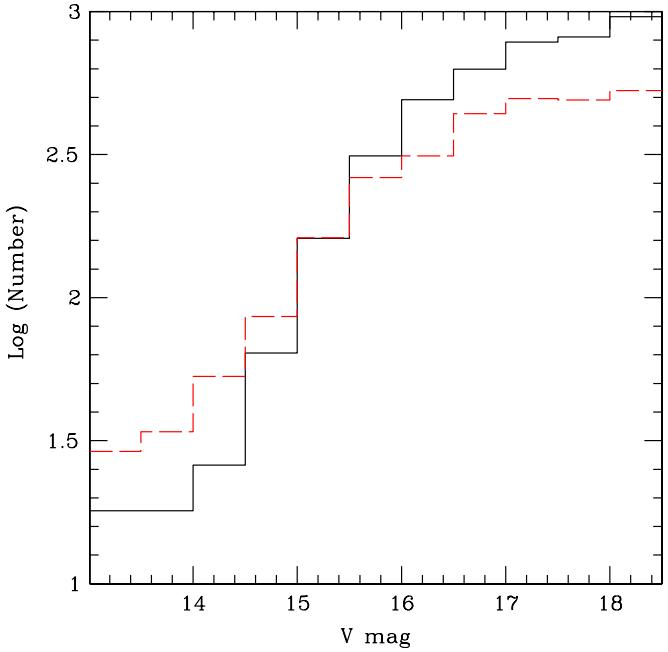

Figure 8. Distribution in magnitude. We compare the magnitudes of the subsample of stars for which we obtained radial velocities (red, dashed histogram) with that of the parent population (black, solid histogram).

(A color version of this figure is available in the online journal.)

where the functional form reflects both errors in the standard star velocities and in uncertainties due to the cross-correlation (see Tonry & Davis 1979). The typical (median) r value for our data is 33, corresponding to a 2.6 km s^{-1} error.

As a further check, in Figure 7 we compare the velocities obtained from the two observations of the Brt5-1 field. We find that there is an excellent match between the observations over all the velocities we have sampled. As mentioned above, this was not the case when we originally used the low-dispersion templates, where we saw a velocity-dependent problem. For all future purposes in the paper, the velocities produced during multiple observations were averaged to yield one Vel_{obs} for each program object. It is clear that a few stars have variable velocities based on this comparison; we expect these stars to be binaries. If two observations of the same star differed by 10 km s^{-1} or more we note this fact in Table 3.

Since we will be using the supergiants we identify to test if the models predict the same relative number with luminosity, we should understand what magnitude biases exist, if any, in the subsample of targets for which we obtained radial velocities compared to the parent sample. In Figure 8, we show the distribution of magnitudes in the complete sample of 4282 objects that met our original criteria (magnitude, color, and location) in black. The red (dashed) histogram shows the sample of 2989 objects for which we successfully obtained radial velocities. We show this on a log plot so that a linear difference corresponds to a percentage; i.e., a difference of 0.3 dex is a factor of 2 regardless of the absolute numbers. We find very good agreement, with only a slight tendency toward having obtained radial velocities for a larger percentage of brighter stars

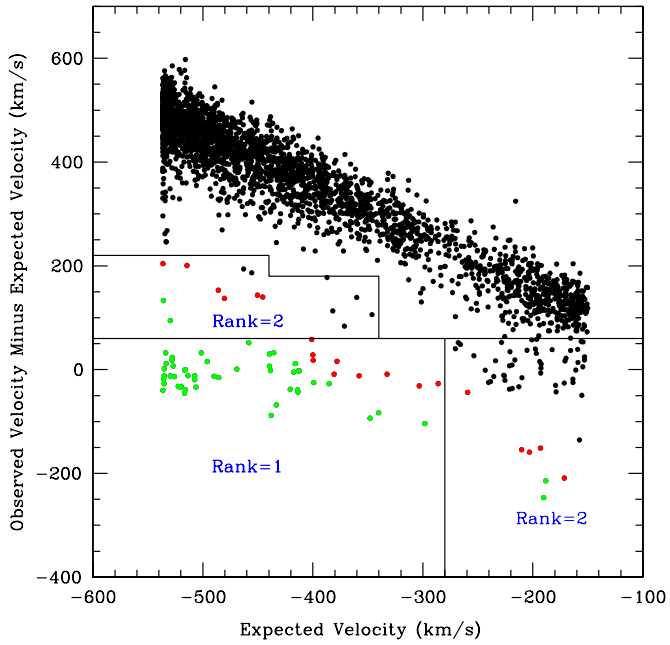

Figure 9. Comparison between the observed and expected radial velocities. Here we plot the difference between the observed and expected radial velocities versus the expected radial velocities. Any M31 members will lie near a difference of 0, while the dark band is composed of foreground dwarfs. Those objects with $V_{\rm obs} \leqslant -400$ km s^{-1} are marked in green and those with -400 km s$^{-1} \leqslant V_{\rm obs} \leqslant -300$ km s^{-1} as red. The assigned "ranks" (1, mostly certain supergiant; 2, probable supergiant) are shown.

(A color version of this figure is available in the online journal.)

than fainter ones. This will introduce a slight bias in our final results in that higher luminosity stars should be proportionally over-represented in our sample.

3.2. Identifying the Supergiants

Now armed with the observed radial velocities of our 2899 program objects, two main steps are necessary to identify the M31 yellow supergiants. First, foreground dwarf contaminants must be eliminated by determining which objects' velocities match that expected from the M31's rotation curve and, second, once a list of M31 members has been obtained, any non-stellar objects (i.e., small clusters) must be removed.

In the notation of Rubin & Ford (1970), the radial velocity V_r of an object in a disk galaxy can be approximated by $V_r = V_0 + V(R) \sin\xi \cos\theta$ where V_0 is the systemic radial velocity, ξ is the angle between the line of sight and the perpendicular to the plane of the galaxy, $V(R)$ is the rotational velocity within the plane at a radial distance R, and $\cos\theta = X/R$ where X is the position along the major axis. This would be a linear relationship only if the rotation curve was absolutely flat, i.e., $V(R)$= const. However, as mentioned in Section 2.1 this is a good approximation for M31. We used the same fit, as described there, to compute what the radial velocity of each of our program objects *should have been* (given its position on the sky) were it an M31 member. The difference between our $V_{\rm obs}$ and $V_{\rm expect}$ for all objects was then calculated and plotted against $V_{\rm expect}$, as shown in Figure 9.

In Figure 9, all the objects whose velocities correspond to the M31's rotation curve should lie along the zero point of the Y-axis. The left-hand side of the plot, where the expected velocities are highly negative, represents the southwestern portion of M31, rotating *toward* the Milky Way. Thus, the strong diagonal band represents the foreground dwarfs (objects with an essentially zero radial velocity). As can be seen, the M31 members can easily be distinguished from the foreground dwarfs on the left side of the plot and the distinction becomes increasingly hazy as we move along the M31's semimajor axis. We therefore distinguish between two "ranks" of M31 members. Rank-1 objects are those which we can say are "nearly certain" M31 members, whereas rank-2 objects we consider to be "probable" M31 members. All objects with an expected velocity < -280 and difference <60 were labeled as rank 1, and those with expected velocity > -280 and difference <60, expected velocity < -340 and difference <180, or expected velocity < -440 and difference <220 were labeled as rank 2. These distinctions are displayed in Figure 9.

As a result of this classification we were left with a list of 56 nearly certain and 71 probable M31 members. There still existed the possibility, however, that some of these M31 members were not stars, but small clusters. This was addressed by measuring the size of the objects as compared to nearby stars. We did this using two methods, both utilizing the images of the LGGS. Initially the 127 potential supergiants were examined with the Source Extractor (Bertin & Arnouts 1996), using the V-band images, and the results were then compared to an independently conducted manual check on the R-band. The manual check was completed by measuring the FWHM of each potential supergiant and its neighbors in the IRAF package imexam. The agreement between the manual and Source Extractor method was complete with each yielding seven previously known (Galleti et al. 2007) clusters in our sample: Mag-237751, J004345.23+410608.5, J004446.42+412918.3, J004545.58+413942.4, J004356.46+412203.3, J004358.15+412438.8, and J004403.98+412618.7.

Once the foreground contaminants and M31 clusters had been removed from our sample and our rank designations are applied, we found that, out of our original sample of 2899 objects, we are left with 54 rank-1 and 66 rank-2 yellow supergiants. This corresponds to a foreground contamination between 96% and 98%! The velocity information for these 120 objects, as well as the seven M31 clusters (listed at the end), is summarized in Table 4.

How clean is our remaining list of candidates? As discussed in Section 1.2 we expect that our original sample to contain some small fraction of Milky Way halo stars in addition to the numerous foreground disk stars. Although the radial velocities are effective at eliminating the disk contaminants, they will be less effective at weeding out the halo stars. Of the ~ -300 km s^{-1} systemic velocity of M31, about two-thirds of it is the reflex motion of the sun: Equation (4) of Courteau & van den Bergh (1999) implies a reflex motion of -178 km s^{-1}. Stars from the halo are therefore likely to reflect this solar motion. If the halo's velocity dispersion is 130 km s^{-1} (Binney & Merrifield 1998), then 3σ velocities could extend all the way to -570 km s^{-1}. If there were a significant number of such stars in our sample, then some contamination could occur.

In Figure 5, we compare our observed velocities (dashed, red histogram) with that expected for foreground stars according to the Besancon model (solid, black histogram). We see that virtually all of the stars with observed velocities greater than -175 km s^{-1} are foreground objects, as expected. At -200 km s^{-1} about half of the objects should be foreground, and half M31. More negative than this, the M31 population dominates, with increasingly little foreground contamination. The detailed output of the Besancon model shows seven foreground stars with

Table 4
Observed Properties of Probable M31 Members

Star	α_{2000}	δ_{2000}	Vel_{obs} (km s^{-1})	r[b]	Vel_{expect} (km s^{-1})	$Vel_{obs}-Vel_{exp}$ (km s^{-1})	V	$B-V$	Rank[c]
J003745.26+395823.6	00:37:45.257	+39:58:23.54	−521.7	20.0	−533.4	11.7	17.16	0.59	1
J003907.59+402628.4	00:39:07.587	+40:26:28.32	−533.6	18.9	−535.1	1.5	16.74	0.86	1
J003922.08+402031.5	00:39:22.077	+40:20:31.42	−504.2	10.0	−527.8	23.6	18.36	0.18	1
J003926.72+402239.4	00:39:26.717	+40:22:39.32	−541.7	8.2	−529.6	−12.1	18.07	0.08	1
J003930.55+403135.2	00:39:30.547	+40:31:35.11	−547.1	30.3	−535.2	−11.9	18.15	0.78	1
J003930.79+401841.1	00:39:30.787	+40:18:41.02	−518.0	19.2	−516.6	−1.4	16.90	0.46	1
J003935.23+401947.7	00:39:35.227	+40:19:47.62	−515.9	20.8	−516.0	0.1	17.92	0.98	1
J003943.43+403524.9	00:39:43.427	+40:35:24.81	−501.6	16.5	−533.8	32.2	17.17	0.23	1
J003948.28+403856.4	00:39:48.277	+40:38:56.30	−519.9	35.4	−527.0	7.1	17.88	0.92	1
J003948.85+403844.8	00:39:48.847	+40:38:44.70	−509.9	25.3	−528.1	18.2	17.40	0.65	1
J003949.86+405305.8	00:39:49.857	+40:53:05.69	−440.3	24.2	−438.6	−1.7	17.34	1.02	1
J003953.55+402827.7	00:39:53.547	+40:28:27.61	−539.5	35.1	−525.9	−13.6	17.45	1.18	1
J004009.13+403142.9	00:40:09.127	+40:31:42.81	−554.8	25.5	−522.4	−32.4	17.63	0.84	1
J004009.70+403719.0	00:40:09.697	+40:37:18.91	−554.4	9.3	−535.7	−18.7	18.27	0.20	1
J004017.72+400436.6	00:40:17.717	+40:04:36.54	−409.1	13.6	−439.4	30.3	18.33	0.26	1
J004020.37+403428.8	00:40:20.367	+40:34:28.71	−554.2	13.4	−520.8	−33.4	18.43	0.24	1
J004021.21+403117.1	00:40:21.207	+40:31:17.01	−527.0	16.6	−507.5	−19.5	16.65	0.28	1
J004021.64+403256.5	00:40:21.637	+40:32:56.41	−525.2	22.9	−513.5	−11.7	17.83	0.51	1
J004025.48+405041.0	00:40:25.477	+40:50:40.89	−469.2	11.7	−501.4	32.2	17.99	0.13	1
J004026.68+403604.4	00:40:26.677	+40:36:04.31	−552.4	7.7	−519.9	−32.5	18.44	0.24	1
J004029.38+403604.2	00:40:29.377	+40:36:04.11	−562.5	17.5	−516.7	−45.8	18.13	0.31	1
J004030.10+402943.1	00:40:30.097	+40:29:43.01	−502.8[d]	8.6	−489.9	−12.9	18.27	0.15	1
J004030.62+404523.8	00:40:30.617	+40:45:23.70	−562.3	18.5	−535.2	−27.1	18.33	0.29	1
J004032.90+404352.8	00:40:32.897	+40:43:52.70	−576.6	32.5	−536.4	−40.2	18.12	0.92	1
J004034.00+405358.3	00:40:33.997	+40:53:58.19	−500.9	20.0	−485.6	−15.3	18.02	0.46	1
J004034.00+403500.1	00:40:33.997	+40:35:00.01	−540.0	19.6	−506.3	−33.7	17.70	0.44	1
J004035.37+405701.0	00:40:35.367	+40:57:00.89	−406.2	7.2	−458.2	52.0	18.11	0.20	1
J004038.10+403827.2	00:40:38.097	+40:38:27.10	−554.5	23.7	−515.9	−38.6	17.59	0.96	1
J004053.97+403256.2	00:40:53.967	+40:32:56.11	−468.0	14.2	−469.1	1.1	18.31	0.80	1
J004101.24+410434.6	00:41:01.237	+41:04:34.48	−427.7	2.4	−416.0	−11.7	17.12	0.92	1
J004101.76+410429.2	00:41:01.757	+41:04:29.08	−422.4	6.7	−417.5	−4.9	17.42	0.82	1
J004102.78+410900.6	00:41:02.777	+41:09:00.47	−362.0	21.2	−378.1	16.1	18.35	0.55	1
J004118.69+403152.0	00:41:18.687	+40:31:51.91	−501.5	8.6	−433.3	−68.2	18.14	0.67	1
J004120.56+403515.4	00:41:20.557	+40:35:15.31	−432.9	22.1	−439.5	6.6	17.10	0.60	1
J004120.99+403453.5	00:41:20.987	+40:34:53.41	−526.1	21.8	−437.9	−88.2	18.13	0.45	1
J004128.74+405224.7	00:41:28.737	+40:52:24.59	−519.3	17.9	−507.5	−11.8	17.79	0.25	1
J004129.31+405102.9	00:41:29.307	+40:51:02.79	−511.5	2.2	−496.1	−15.4	16.87	0.72	1
J004131.50+403917.8	00:41:31.497	+40:39:17.70	−403.1	17.2	−435.6	32.5	17.96	0.56	1
J004143.45+403956.4	00:41:43.447	+40:39:56.30	−458.6	21.4	−420.6	−38.0	18.00	0.41	1
J004144.76+402808.9	00:41:44.757	+40:28:08.81	−342.9	20.0	−401.1	58.2	18.29	1.03	1
J004149.87+412712.7	00:41:49.867	+41:27:12.56	−313.0	6.6	−286.1	−26.9	17.99	0.83	1
J004156.90+412109.0	00:41:56.897	+41:21:08.86	−334.8	19.2	−303.3	−31.5	17.17	0.54	1
J004201.09+403951.9	00:42:01.087	+40:39:51.80	−424.2	16.1	−399.2	−25.0	18.46	0.36	1
J004207.22+405148.3	00:42:07.217	+40:51:48.19	−415.8	27.0	−413.3	−2.5	17.02	0.97	1
J004207.85+405152.4	00:42:07.847	+40:51:52.29	−414.8	18.5	−412.3	−2.5	16.99	0.76	1
J004212.20+405513.9	00:42:12.197	+40:55:13.79	−453.0	16.4	−413.9	−39.1	18.24	0.23	1
J004214.85+405652.0	00:42:14.847	+40:56:51.89	−457.0	15.2	−413.6	−43.4	17.97	0.19	1
J004215.06+405148.3	00:42:15.057	+40:51:48.19	−381.5	10.1	−399.7	18.2	18.48	0.88	1
J004226.53+410123.9	00:42:26.527	+41:01:23.78	−371.7	11.6	−400.0	28.3	18.37	0.47	1
J004229.30+405727.6	00:42:29.297	+40:57:27.49	−412.1	9.8	−385.2	−26.9	17.63	0.43	1
J004233.76+410014.6	00:42:33.757	+41:00:14.48	−389.6	24.7	−380.7	−8.9	18.03	0.68	1
J004247.25+410039.2	00:42:47.247	+41:00:39.08	−370.0	9.9	−358.0	−12.0	18.21	0.80	1
J004259.95+410220.3	00:42:59.947	+41:02:20.18	−423.3	4.4	−340.2	−83.1	17.41	1.06	1
J004304.89+410345.9	00:43:04.887	+41:03:45.78	−341.5	11.6	−332.5	−9.0	18.07	0.89	1
J003711.98+395445.2	00:37:11.977	+39:54:45.15	−331.9	18.8	−536.3	204.4	18.06	0.56	2
J003725.57+400731.9	00:37:25.567	+40:07:31.83	−435.2	10.4	−529.7	94.5	18.47	0.50	2
J003934.02+404714.2	00:39:34.017	+40:47:14.10	−269.1	24.8	−463.0	193.9	17.21	0.60	2
J003936.96+400743.8	00:39:36.957	+40:07:43.73	−343.0	11.8	−480.4	137.4	18.19	0.80	2
J003937.44+394941.1	00:39:37.437	+39:49:41.05	−305.7	10.5	−445.6	139.9	17.50	0.46	2
J003942.35+404031.8	00:39:42.347	+40:40:31.70	−313.9	13.0	−514.5	200.6	18.15	0.54	2
J003955.87+401636.4	00:39:55.867	+40:16:36.33	−332.8	23.7	−486.0	153.2	18.43	0.54	2
J004002.91+400659.2	00:40:02.907	+40:06:59.13	−268.9	9.8	−455.6	186.7	17.98	0.40	2
J004007.14+410321.8	00:40:07.137	+41:03:21.68	−209.5	18.1	−387.1	177.6	18.08	0.54	2
J004020.37+410723.2	00:40:20.367	+41:07:23.08	−287.6	15.1	−371.3	83.7	18.32	0.68	2
J004034.82+401825.5	00:40:34.817	+40:18:25.42	−306.9	23.4	−450.4	143.5	16.30	0.61	2
J004107.40+405328.6	00:41:07.397	+40:53:28.49	−402.7	14.2	−535.9	133.2	17.50	0.47	2

Table 4
(Continued)

Star	α_{2000}	δ_{2000}	Vel_{obs} (km s^{-1})	r[b]	Vel_{expect} (km s^{-1})	$Vel_{obs}-Vel_{exp}$ (km s^{-1})	V	$B-V$	Rank[c]
J004148.69+413814.1	00:41:48.687	+41:38:13.95	−215.7	27.5	−267.8	52.1	18.49	0.63	2
J004217.15+403740.2	00:42:17.147	+40:37:40.11	−268.7	36.1	−381.9	113.2	17.77	0.66	2
J004223.21+412803.2	00:42:23.207	+41:28:03.06	−303.0	17.5	−259.3	−43.7	18.36	0.67	2
J004231.84+412039.9	00:42:31.837	+41:20:39.76	−230.1	16.1	−270.4	40.3	18.44	0.55	2
J004232.90+412103.4	00:42:32.897	+41:21:03.26	−217.4	27.2	−265.9	48.5	17.43	0.86	2
J004235.91+413050.6	00:42:35.907	+41:30:50.45	−265.0	11.8	−240.3	−24.7	17.80	0.47	2
J004237.52+413024.8	00:42:37.517	+41:30:24.65	−261.4	11.9	−238.5	−22.9	17.33	0.24	2
J004240.34+412807.2	00:42:40.337	+41:28:07.06	−248.9	15.1	−235.5	−13.4	18.01	0.52	2
J004243.54+414620.6	00:42:43.537	+41:46:20.44	−176.1	34.8	−228.5	52.4	17.20	0.74	2
J004245.97+414422.1	00:42:45.967	+41:44:21.94	−237.3	12.9	−226.5	−10.8	17.99	0.18	2
J004247.30+414451.0	00:42:47.297	+41:44:50.84	−246.1	17.6	−225.4	−20.7	16.41	0.47	2
J004248.11+403434.5	00:42:48.107	+40:34:34.41	−220.8	28.5	−360.1	139.3	17.20	0.76	2
J004250.67+414008.6	00:42:50.667	+41:40:08.44	−259.1	27.9	−221.3	−37.8	17.85	0.67	2
J004251.90+413745.9	00:42:51.897	+41:37:45.75	−210.1	30.5	−218.9	8.8	14.98	0.62	2
J004252.87+412328.6	00:42:52.867	+41:23:28.46	−181.4	13.9	−192.5	11.1	18.30	0.09	2
J004255.16+413515.3	00:42:55.157	+41:35:15.15	−245.6	19.1	−212.7	−32.9	17.84	0.83	2
J004259.62+413946.1	00:42:59.617	+41:39:45.94	−364.6	12.7	−210.2	−154.4	18.48	0.49	2
J004301.96+405315.2	00:43:01.957	+40:53:15.09	−240.3	31.0	−346.2	105.9	17.78	0.79	2
J004302.55+413332.0	00:43:02.547	+41:33:31.85	−138.3	52.1	−196.6	58.3	17.87	0.75	2
J004303.69+414543.3	00:43:03.687	+41:45:43.14	−225.5	13.1	−209.9	−15.6	18.21	0.22	2
J004311.34+414240.9	00:43:11.337	+41:42:40.74	−158.0	31.1	−197.7	39.7	18.17	0.79	2
J004313.02+414144.9	00:43:13.017	+41:41:44.74	−178.1	35.5	−193.8	15.7	16.97	0.63	2
J004314.47+414229.1	00:43:14.467	+41:42:28.94	−199.5	10.7	−192.9	−6.6	18.13	0.10	2
J004318.57+415311.1	00:43:18.567	+41:53:10.93	−143.7	59.9	−201.0	57.3	16.54	0.78	2
J004325.93+413910.6	00:43:25.927	+41:39:10.45	−182.0	48.2	−163.6	−18.4	18.32	0.75	2
J004337.16+412151.0	00:43:37.157	+41:21:50.86	−221.6	23.5	−178.8	−42.8	17.02	0.91	2
J004338.76+414915.1	00:43:38.757	+41:49:14.94	−197.5	8.5	−171.5	−26.0	18.16	0.26	2
J004348.01+415406.2	00:43:48.007	+41:54:06.03	−148.1	31.4	−169.9	21.8	18.30	0.59	2
J004406.32+420131.3	00:44:06.317	+42:01:31.12	−188.3	19.2	−163.5	−24.8	15.60	0.46	2
J004409.23+415941.1	00:44:09.227	+41:59:40.93	−102.0	37.1	−156.1	54.1	17.42	0.62	2
J004409.98+420121.1	00:44:09.977	+42:01:20.92	−145.1	23.5	−159.0	13.9	17.42	0.60	2
J004410.62+411759.7	00:44:10.617	+41:17:59.57	−244.5	21.1	−243.3	−1.2	17.63	0.40	2
Mag-253496	00:44:12.450	+41:16:08.42	−226.9	54.5	−253.6	26.7	15.15	1.18	2
J004424.21+412116.0	00:44:24.207	+41:21:15.86	−238.0	14.3	−225.9	−12.1	16.73	0.91	2
J004427.76+412209.8	00:44:27.757	+41:22:09.66	−213.9	19.9	−221.3	7.4	17.26	1.03	2
J004428.99+412010.7	00:44:28.987	+41:20:10.56	−216.8	9.1	−233.9	17.1	17.80	0.31	2
J004432.01+412442.0	00:44:32.007	+41:24:41.86	−168.2	5.4	−205.3	37.1	18.28	0.07	2
J004432.41+412947.5	00:44:32.407	+41:29:47.35	−120.2	59.4	−159.3	39.1	17.05	0.73	2
J004440.60+412704.1	00:44:40.597	+41:27:03.96	−189.8	27.8	−192.7	2.9	18.22	1.33	2
J004441.56+412636.6	00:44:41.557	+41:26:36.46	−165.4	9.3	−196.9	31.5	17.96	0.44	2
J004444.50+412314.3	00:44:44.497	+41:23:14.16	−186.3	40.6	−220.8	34.5	17.57	0.65	2
J004447.45+412409.7	00:44:47.447	+41:24:09.56	−197.9	12.3	−216.4	18.5	18.10	0.22	2
J004458.01+413217.5	00:44:58.007	+41:32:17.35	−128.8	11.6	−165.7	36.9	17.79	0.17	2
J004508.90+413117.8	00:45:08.897	+41:31:17.65	−144.0	32.6	−182.5	38.5	17.12	0.61	2
J004509.86+413031.5	00:45:09.857	+41:30:31.35	−402.6	6.3	−188.3	−214.3	16.83	0.56	2
J004518.17+413615.6	00:45:18.167	+41:36:15.45	−101.1	41.2	−154.4	53.3	17.84	0.68	2
J004518.76+413630.7	00:45:18.757	+41:36:30.55	−128.4	19.5	−153.1	24.7	16.70	0.51	2
J004526.93+412613.6	00:45:26.927	+41:26:13.46	−255.0	24.6	−218.8	−36.2	18.45	0.75	2
J004532.62+413227.8	00:45:32.617	+41:32:27.65	−436.7	35.3	−190.2	−246.5	15.79	0.85	2
J004535.23+413600.5	00:45:35.227	+41:36:00.35	−154.3	75.8	−170.8	16.5	15.88	0.94	2
J004554.48+413359.8	00:45:54.477	+41:33:59.65	−344.4	20.1	−193.1	−151.3	17.16	0.59	2
J004559.84+414038.2	00:45:59.837	+41:40:38.04	−161.9	5.9	−161.0	−0.9	17.71	0.22	2
J004618.59+414410.9	00:46:18.587	+41:44:10.74	−149.2	34.8	−154.6	5.4	15.22	0.65	2
J004658.64+414948.4	00:46:58.637	+41:49:48.24	−134.6	15.0	−153.1	18.5	18.30	0.48	2
Mag-237751	00:41:01.181	+41:13:45.83	−441.5	41.1	−348.0	−93.5	14.13	1.12	Cl
J004345.23+410608.5	00:43:45.227	+41:06:08.38	−402.1	28.3	−298.2	−103.9	18.32	0.52	Cl
J004356.46+412203.3	00:43:56.457	+41:22:03.16	−362.0	59.1	−203.1	−158.9	16.88	0.08	Cl
J004358.15+412438.8	00:43:58.147	+41:24:38.66	−380.4	47.9	−171.4	−209.0	17.35	0.99	Cl
J004403.98+412618.7	00:44:03.977	+41:26:18.56	−293.1	26.5	−157.6	−135.5	18.17	0.71	Cl
J004446.42+412918.3	00:44:46.417	+41:29:18.16	−209.8	63.5	−179.4	−30.4	17.96	0.26	Cl
J004545.58+413942.4	00:45:45.577	+41:39:42.25	−204.9	48.5	−155.5	−49.4	18.13	0.89	Cl

Notes.
[a] Tonry & Davis (1979) r parameter.
[b] Rank: 1, highly likely supergiant; 2, probable supergiant; 3, dwarf; Cl, cluster.
[c] Radial velocity observed on two different nights differed by 10 km s^{-1} or more.

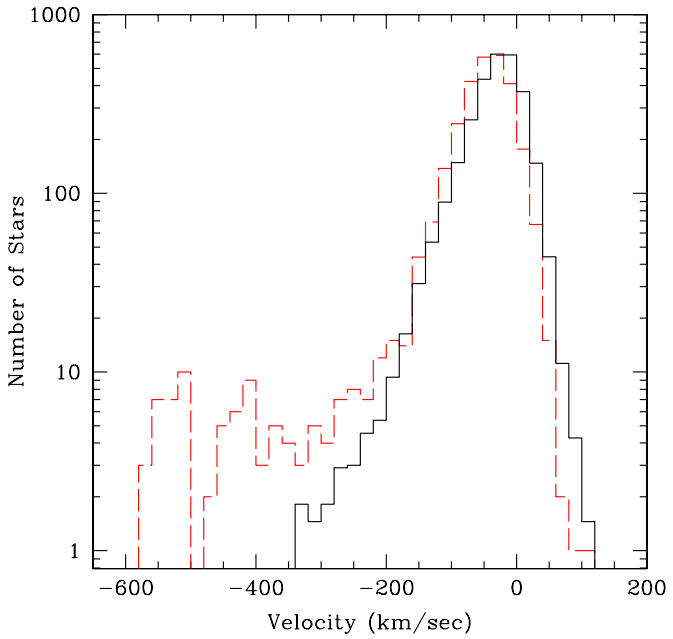

Figure 10. Histogram of radial velocities. The observed radial velocities (red, dashed histogram) are compared with those we expect for the foreground contamination (black, solid histogram) computed from the Bescancon model. (A color version of this figure is available in the online journal.)

radial velocities $\leqslant -300$ km s^{-1}, and one foreground star with a radial velocity $\leqslant -400$ km^{-1}.

We can also estimate this contamination independently using the Bahcall & Soneira (1980) model which predicts about 40 halo dwarfs per square degree within the magnitude and color range we use in the direction of M31. As for halo *giants*, the Bahcall & Soneira (1980) model overestimates their number (Morrison 1993), but H. Morrison (2008, private communication) has been kind enough to calculate that there should be about four such objects in a square degree seen toward M31 in this same magnitude and color range. The effective area in our survey is about 1 deg^2, and in it we observed 68% of the stars in our original sample, so we might realistically expect about 30 halo stars in our spectroscopic sample. Assuming the radial velocity distribution is Gaussian, this leads to the identical results as above: there should be five halo stars with velocities more negative than -300 km s^{-1} (0.94σ) and 1 below -400 km s^{-1} (1.8σ).

So, simply noting that the rank-1 stars all have velocities more negative than -280 km s^{-1}, we expect *at most* eight stars in this sample of 54, or 15%. However, this is likely to be an overestimate of the contamination, as it ignores the additional information gained by the star's position and therefore its *expected* radial velocity, $V_{\rm expect}$, were it an M31 member. To be a rank-1 candidate, a star has to be in the right location within the M31 field such that its $V_{\rm obs}$ corresponds to its $V_{\rm expect}$ (which, although still possible, is improbable). We therefore refer to the rank-1 candidates as "nearly certain." The situation for the rank-2 candidates is harder to evaluate, as a few of these have radial velocities as positive as -100 km s^{-1}, but their location in the Figure 9 leads us to consider them "probable" yellow supergiants. Contamination by foreground stars of half of this sample would not surprise us, however.

Of our original 2899 program objects, four had previously appeared in the literature as spectroscopically confirmed members of M31. J003745.26+395823.6 appeared in Humphreys (1979) as IV-A207 and was classified as F5 Ia, J004101.24+410434.6 can be found by the name OB69-46 in Massey (1998a) as an RSG (based on the earlier photometry), and J004129.31+405102.9 is listed as OB22A in Humphreys et al. (1990) and classified as a F8-G0 Ia. We categorized all three as rank-1 yellow supergiants. Additionally, Humphreys et al. (1988) list J004101.55+403432.3 (as III-R61) as an M31 RSG (K5 I) candidate. However, we are forced to conclude that this star is actually a foreground dwarf, given its -41 km s^{-1} radial velocity (at its position in M31, the expected radial velocity is -464 km s^{-1}. We have double checked our previous cross-identification of this star, and it matches the one shown on the Humphreys et al. (1988) finding chart; the colors $B-V=0.69$ and $U-B=0.02$ do not correspond to mid-K-type, and the spectrum is clearly of earlier type, with the Balmer lines prominent, along with strong lines of Mg I and Fe I.

3.3. Physical Properties: Transforming the Photometry

In order to use our list of M31 yellow supergiants to test the current stellar evolutionary tracks, it is necessary to determine their effective temperatures and bolometric luminosities. For this, we will transform each star's photometry, as described below.

The B and V photometries for all but one of our stars came from the LGGS; that of the single "bright" star, Mag-253496 is taken from Magnier et al. (1992) and adjusted by the small correction found by Massey et al. (2006). We apply a constant reddening correction $E(B-V)=0.13$ based on the median value found for early-type stars in M31 by Massey et al. (2007b), and is in accord with the color excess derived from spectral types of a handful of O-type stars (Massey et al. 1986). The reddening of individual stars can readily differ from this (by several tenths) but in this part of the CMD reddening-free indices such as Q are degenerate with $T_{\rm eff}$, as one may note in Figure 4, the reddening vector is nearly parallel to the supergiant sequence.

The problem now becomes how to best translate these dereddened colors into effective temperatures. Flower (1996) and Kovtyukh (2007) both present empirical effective temperature scales that include F- and G-type supergiants. The Flower (1996) data are drawn from the literature, while Kovtyukh (2007) performs his own analysis on spectra of Galactic supergiants. The problem is that both of these studies are based upon samples of Galactic supergiants, while we expect the metallicity of our M31 stars to be about 2× solar based upon H II region abundances (i.e., Zaritsky et al. 1994). We therefore have decided to instead use the Kurucz (1992) "Atlas9" model atmospheres to provide the transformations.

In Figure 11, we compare the Altas9 models for solar metallicity with the two empirical calibrations.[9] For this comparison, we have used the lowest two surface gravities for each temperature model computed by Kurucz (1992), i.e., $\log g=0.0$ and 0.5 for $T_{\rm eff}\leqslant 6000$ K, $\log g=0.5$ and 1.0 for 6250 K$\leqslant T_{\rm eff}<$ 7500 K, and $\log g=1.0$ and 1.5 for 7500 K$\leqslant T_{\rm eff}\leqslant 8500$ K. For the purposes of comparing our data to the stellar evolutionary models, we will restrict ourselves only to our defined yellow supergiant effective temperature range: 7500 K–4800 K ($\log T_{\rm eff}=3.875$ and 3.681). This region is indicated by the two horizontal lines in Figure 11. We can see that over this temperature range there is substantial agreement between the models and the empirical calibrations.

[9] We have used the intrinsic colors of FitzGerald (1970) as a function of spectral types in order to assign $(B-V)_0$ values to the spectral types given by Kovtyukh (2007).

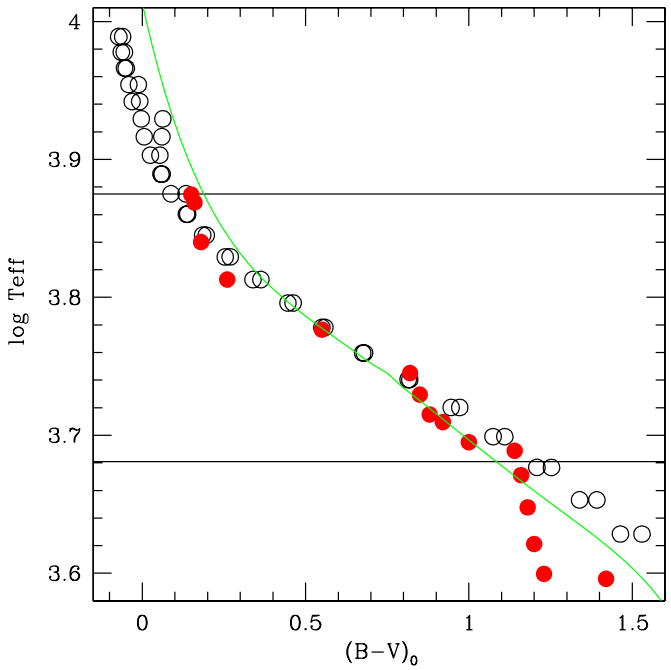

Figure 11. Comparison of effective temperature scales. The Atlas9 model predictions are shown by open (black) circles for surface gravities appropriate to supergiants. The filled (red) circles are from the Kovtyukh (2007) study of F- and G-type supergiants. The solid (green) curve is the Flower (1996) relation for supergiants. the two horizontal lines correspond to effective temperatures of 7500 K and 4800 K, the region we consider the realm of the yellow supergiants here.

(A color version of this figure is available in the online journal.)

As mentioned above, one advantage of using the Atlas9 models is that we can fine-tune the transformations to an appropriate metallicity, although we will find below that this correction is very slight. In keeping with Zaritsky et al. (1994) we assume an M31 metallicity of 2× solar (see further discussion in Crockett et al. 2006 and Massey et al. 2009). Using the Atlas9 model with the most similar metallicity (1.6× solar) we compute a relationship between $(B-V)_0$ and $\log T_{\rm eff}$ as follows:

$$\log T_{\rm eff} = 3.913 - 0.3512(B-V)_0 + 0.2692(B-V)_0^2 - 0.1108(B-V)_0^3.$$

To keep the relationship accurate over the range of temperatures in which we are the most interested, we restricted the fit to models that just bracketed the temperature range above (i.e., Kurucz models with 4750 K $\leqslant T_{\rm eff} \leqslant$ 8000 K), and therefore this relationship is *only* applicable for $0.03 \leqslant (B-V)_0 \leqslant 1.26$. Since we adopted an average value of $E(B-V) = 0.13$, this then corresponds to $0.16 \leqslant B-V \leqslant 1.39$, a good match to the $0.0 \leqslant B-V \leqslant 1.4$ of our sample. Only six stars of our 120 yellow supergiants have colors bluer than $B-V = 0.16$. Although we will not include these in our comparison to the evolutionary models in the next section, we nevertheless would like to include these in the HRD, and so we will adopt the following approximate transformation for these stars: $\log T_{\rm eff} = 3.934 - 0.549(B-V)_0$.

The bolometric corrections are relatively modest for yellow supergiants (a few tenths of a magnitude), and we derive the following relationship using the Atlas9 models; the results are valid between 4750 K and 9500 K, and, hence, applicable to our complete sample:

$$\mathrm{BC} = -251.54 + 130.763 \log T_{\rm eff} - 16.9934(\log T_{\rm eff})^2.$$

How much difference does adopting 1.6× solar metallicity make? The difference is slight: for a star with $(B-V)_0 = 0.6$ (roughly corresponding to 6000 K) we would derive $\log T_{\rm eff} = 3.775$ using the 1.6× Atlas9 relationship given above, while we would derive $\log T_{\rm eff} = 3.769$ from an analogous relationship derived from the 1.0× models. The difference, 0.006 dex, is negligible.

We give the derived physical properties in Table 5 for the 120 probable supergiants sorted by bolometric luminosities. A distance modulus of 24.40 (0.76 Mpc) was adopted, following the discussion in van den Bergh (2000).

3.4. Membership Re-examined

One of the critical and interesting properties we are attempting to determine is the upper luminosity limit for yellow supergiants, and we were struck by the fact that the ten most luminous stars in Table 5 were all of rank 2. We argue above that we expect some (minimal) contamination by foreground (halo) giants in our sample, as these stars would have radial velocities characteristic of the reflex motion of the Sun. In particular, the three most luminous possible supergiants stand out as extraordinarily bright. None of the three have extreme radial velocities (which is in part why they are rank "2"): Mag-253496 has a $\mathrm{Vel_{obs}}$ of −227 km s^{-1}; J004251.90+413745.9 has a $\mathrm{Vel_{obs}}$ of −210 km s^{-1}; and J004618.59+414410.9 has a $\mathrm{Vel_{obs}}$ of −150 km s^{1}, as can be seen in Table 4. We were therefore very keen to confirm or refute their membership in M31. The wavelength range of our own spectra had been optimized for radial velocities and where Hectospec has good throughput, and did not include the various good luminosity indicators in the far blue (see below) nor the O I λ7774 triplet in the far red.

The Kitt Peak Director was sympathetic to our plight and arranged follow-up spectra to be obtained for these three stars plus comparison spectral standards. The data were obtained as part of engineering time on the 3.5 m WIYN telescope with the Hydra fiber spectrometer in the far red, and on the Kitt Peak 4 m Mayall telescope with the Ritchey–Chrétien (RC) spectrograph (in the blue). These spectra convinced us that all three of these are actually halo stars, and not M31 supergiants, as we argue below; they also eliminated another rank-2 star from membership, and confirmed the membership of other (both rank-1 and rank-2) stars.

The WIYN Hydra spectra were obtained on 2008 August 11, and consisted of an 1800 s exposure and a 1300 s exposure; the latter was ended due to clouds. The setup included Mag-253496 and J004251.90+413745.9 and a number of other stars, but not J004618.59+414410.9. The (2.8 pixel) resolution was 4.0 Å. The wavelength range included the O I λ7774 triplet, known to have a strong luminosity effect in F-type supergiants (Osmer 1972) due to non-LTE effects, exacerbated by sphericity and the large mass outflows found in supergiants (Przybilla et al. 2000). We include in Table 5 that we find for this line. The two most luminous supergiant candidates have little or no O I λ7774, arguing they cannot be supergiants, and we identify another non-supergiant among the rank-2 objects we observed. Strong O I λ7774 is found for several of the other rank-1 and rank-2 candidates.

The 4 m RC spectrograph spectra were obtained on 2008 September 4, and consisted of a 3 × 900 s exposure of Mag-253496, and 3 × 500 s exposures of J004251.90+413745.9 and J004618.59+414410.9. The wavelength region included 3880–4600 Å at a (2.2 pixel) resolution of 1.6 Å. Several spectral standards were also observed to provide guidance

Table 5
Derived Properties of Potential M31 Supergiants

Star	Rank	M_V	$T_{\rm eff}$	$\log(L/L_\odot)$	Comment
Mag-253496	2	(−9.65)	(3.713)	(5.87)	No O I λ7774–Non-member
J004251.90+413745.9	2	(−9.82)	(3.792)	(5.84)	No O I λ7774–Non-member
J004618.59+414410.9	2	(−9.58)	(3.787)	(5.75)	Non-member
J004406.32+420131.3	2	−9.20	3.822	5.58	
J004532.62+413227.8	2	−9.01	3.758	5.55	
J004535.23+413600.5	2	−8.92	3.746	5.53	Strong O I λ7774
J004034.82+401825.5	2	−8.50	3.794	5.31	
J004247.30+414451.0	2	−8.39	3.821	5.25	Very strong O I λ7774
J004318.57+415311.1	2	−8.26	3.768	5.24	
J004424.21+412116.0	2	−8.07	3.750	5.18	Strong O I λ7774
J003907.59+402628.4	1	−8.06	3.757	5.17	
J004021.21+403117.1	1	−8.15	3.867	5.15	
J004518.76+413630.7	2	−8.10	3.812	5.14	
J004129.31+405102.9	1	−7.93	3.776	5.10	
J004509.86+413031.5	2	(−7.97)	(3.804)	(5.09)	Weak O I λ7774–Non-member?
J004207.22+405148.3	1	−7.77	3.743	5.08	
J004337.16+412151.0	2	−7.78	3.750	5.07	Strong O I λ7774
J004207.85+405152.4	1	−7.81	3.771	5.06	
J003930.79+401841.1	1	−7.90	3.823	5.05	
J004313.02+414144.9	2	−7.83	3.791	5.04	
J004101.24+410434.6	1	−7.68	3.749	5.03	
J004432.41+412947.5	2	−7.75	3.776	5.03	
J004120.56+403515.4	1	−7.70	3.796	4.99	
J004427.76+412209.8	2	−7.54	3.734	4.99	
J004508.90+413117.8	2	−7.68	3.794	4.98	
J004248.11+403434.5	2	−7.59	3.771	4.97	
J004243.54+414620.6	2	−7.60	3.774	4.97	
J003949.86+405305.8	1	−7.46	3.736	4.96	
J004554.48+413359.8	2	−7.64	3.797	4.96	
J004156.90+412109.0	1	−7.63	3.807	4.96	Very strong O I λ7774
J003745.26+395823.6	1	−7.64	3.797	4.96	
J003943.43+403524.9	1	−7.63	3.879	4.95	
J003953.55+402827.7	1	−7.35	3.712	4.95	
J003934.02+404714.2	2	−7.59	3.795	4.94	
J004259.95+410220.3	1	−7.39	3.730	4.94	
J004101.76+410429.2	1	−7.38	3.762	4.89	
J004237.52+413024.8	2	−7.47	3.877	4.89	
J004232.90+412103.4	2	−7.37	3.756	4.89	
J003948.85+403844.8	1	−7.40	3.787	4.88	
J004409.98+420121.1	2	−7.38	3.796	4.86	
J004409.23+415941.1	2	−7.38	3.793	4.86	
J004038.10+403827.2	1	−7.21	3.743	4.85	
J003937.44+394941.1	2	−7.30	3.823	4.82	
J004107.40+405328.6	2	−7.30	3.821	4.81	
J004444.50+412314.3	2	−7.23	3.787	4.81	
J004009.13+403142.9	1	−7.17	3.760	4.81	
J004410.62+411759.7	2	−7.17	3.835	4.76	
J004229.30+405727.6	1	−7.17	3.830	4.76	
J004301.96+405315.2	2	−7.02	3.767	4.74	
J004559.84+414038.2	2	−7.09	3.884	4.74	
J004217.15+403740.2	2	−7.03	3.787	4.73	
J004255.16+413515.3	2	−6.96	3.761	4.73	
J004034.00+403500.1	1	−7.10	3.827	4.73	
J003935.23+401947.7	1	−6.88	3.741	4.72	
J003948.28+403856.4	1	−6.92	3.750	4.72	
J004458.01+413217.5	2	−7.01	3.898	4.71	
J004440.60+412704.1	2	−6.58	3.688	4.70	
J004250.67+414008.6	2	−6.95	3.785	4.70	
J004302.55+413332.0	2	−6.93	3.773	4.70	
J004518.17+413615.6	2	−6.95	3.783	4.70	
J004128.74+405224.7	1	−7.01	3.876	4.70	Very strong O I λ7774
J004428.99+412010.7	2	−7.00	3.857	4.69	
J004021.64+403256.5	1	−6.97	3.813	4.69	
J004235.91+413050.6	2	−7.00	3.820	4.69	
J003926.72+402239.4	1	−6.73	3.961	4.67	
J004149.87+412712.7	1	−6.81	3.761	4.66	

Table 5
(Continued)

Star	Rank	M_V	$T_{\rm eff}$	$\log(L/L_\odot)$	Comment
J004025.48+405041.0	1	−6.81	3.932	4.66	
J004214.85+405652.0	1	−6.83	3.891	4.64	
J004131.50+403917.8	1	−6.84	3.803	4.64	
J004304.89+410345.9	1	−6.73	3.753	4.64	
J004441.56+412636.6	2	−6.84	3.827	4.63	
J004245.97+414422.1	2	−6.81	3.896	4.63	Strong O I λ7774
J004314.47+414229.1	2	−6.67	3.951	4.63	
J004032.90+404352.8	1	−6.68	3.749	4.63	
J004233.76+410014.6	1	−6.77	3.783	4.63	Very strong O I λ7774
J004002.91+400659.2	2	−6.82	3.836	4.62	
J004240.34+412807.2	2	−6.79	3.810	4.62	
J004034.00+405358.3	1	−6.78	3.823	4.61	Strong O I λ7774
J004143.45+403956.4	1	−6.80	3.833	4.61	
J003711.98+395445.2	2	−6.74	3.803	4.60	
J003930.55+403135.2	1	−6.65	3.769	4.59	
J004432.01+412442.0	2	−6.52	3.966	4.59	
J004311.34+414240.9	2	−6.63	3.767	4.59	
J004007.14+410321.8	2	−6.72	3.807	4.59	
J004035.37+405701.0	1	−6.69	3.888	4.58	
J003936.96+400743.8	2	−6.61	3.765	4.58	
J004144.76+402808.9	1	−6.51	3.734	4.58	
J004118.69+403152.0	1	−6.66	3.784	4.58	
J004447.45+412409.7	2	−6.70	3.882	4.58	
J004247.25+410039.2	1	−6.59	3.765	4.57	
J004252.87+412328.6	2	−6.50	3.954	4.57	
J004029.38+403604.2	1	−6.67	3.857	4.56	
J003942.35+404031.8	2	−6.65	3.806	4.56	
J004120.99+403453.5	1	−6.67	3.825	4.56	
J004338.76+414915.1	2	−6.64	3.871	4.55	
J004303.69+414543.3	2	−6.59	3.884	4.54	
J004030.10+402943.1	1	−6.53	3.924	4.54	
J004053.97+403256.2	1	−6.49	3.766	4.53	
J004325.93+413910.6	2	−6.48	3.773	4.52	
J004212.20+405513.9	1	−6.56	3.881	4.52	
J004020.37+410723.2	2	−6.48	3.783	4.51	
J004348.01+415406.2	2	−6.50	3.797	4.51	
J004009.70+403719.0	1	−6.53	3.889	4.51	
J004658.64+414948.4	2	−6.50	3.819	4.50	
J004223.21+412803.2	2	−6.43	3.785	4.49	
J004030.62+404523.8	1	−6.47	3.864	4.48	Strong O I λ7774
J004017.72+400436.6	1	−6.47	3.873	4.48	
J004102.78+410900.6	1	−6.45	3.806	4.48	
J004215.06+405148.3	1	−6.32	3.754	4.48	
J003922.08+402031.5	1	−6.44	3.897	4.48	
J004226.53+410123.9	1	−6.43	3.820	4.47	
J004526.93+412613.6	2	−6.35	3.772	4.47	
J004231.84+412039.9	2	−6.36	3.804	4.45	
J003955.87+401636.4	2	−6.37	3.807	4.45	
J004026.68+403604.4	1	−6.36	3.878	4.44	
J004020.37+403428.8	1	−6.37	3.876	4.44	
J004148.69+413814.1	2	−6.31	3.790	4.44	
J004201.09+403951.9	1	−6.34	3.845	4.43	Strong O I λ7774
J004259.62+413946.1	2	−6.32	3.816	4.43	
J003725.57+400731.9	2	−6.33	3.815	4.43	

in interpreting the data; these were supplemented by similar data obtained at later data with the Kitt Peak 2.1 m Goldcam spectrometer at a similar dispersion. These data show that Mag-253496 is roughly of spectral type G8, based upon the Fe I λ4143/Hδ and Fe I λ4045/Hδ ratios (Keenan & McNeil 1976). J004251.90+413745.9 and J004618.59+414410.9 are of earlier type, between F5 and G2, based upon the strength of the *G*-band compared to Hγ, and we adopt an F8 type.

For the G8 star, Mag-253496, we find that the ratio of Sr II λ4077 to the Fe II/III blend at λ4063 is about 1, typical of an G8 III; in a supergiant, this ratio would be considerably larger (e.g., Keenan & McNeil 1976). Similarly, the ratio of the Fe, SrII blend at λ4216 to the Ca II λ4226 is quite small, consistent with that of a dwarf or a giant, but not a supergiant. Combined with the lack of O I λ7774, we therefore conclude that this star is a Milky Way halo giant, and not an M31 supergiant.

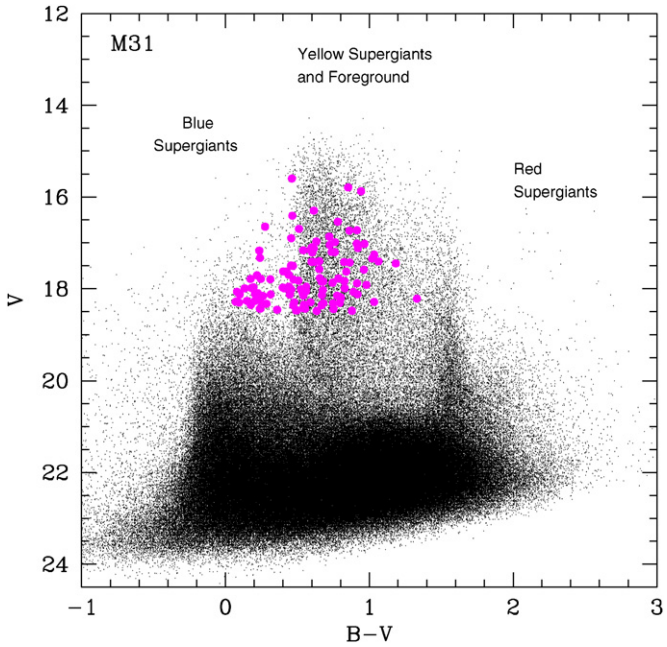

Figure 12. CMD revisited. Same as Figure 1, but the addition of the newly confirmed yellow supergiants marked as colored filled circles.
(A color version of this figure is available in the online journal.)

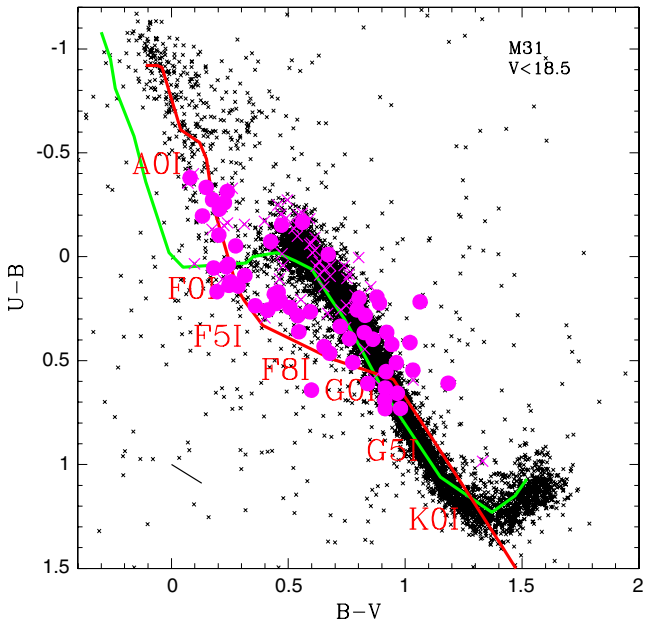

Figure 13. Two-color diagram revisited. Same as Figure 4 (left), but with the yellow supergiants from this paper now marked by filled circles (if rank 1 or spectroscopically confirmed rank 2) or as x's (if unconfirmed rank 2).
(A color version of this figure is available in the online journal.)

For the F8 stars, we find that the strengths of Ti II λ4444 and Mg II λ4481 to be roughly equal, consistent with a giant, but inconsistent with a supergiant. Add to that the lack of O I λ7774 in J004618.59+414410.9, and we conclude that these are also halo giants.

We also include in Table 5 the results of six other stars for which previous spectroscopy by one of us (N. C.) had identified strong O I λ7774. Five of these are rank 1, and one is rank 2. (An additional two stars, one of rank 1 and one of rank 2, were in common with the WIYN spectroscopy, and agreed with our assessment.) These were all obtained with Hectospec using a lower resolution (5 Å) grating as part of a different project (Caldwell et al. 2009). In the following, we consider all stars found to have strong O I λ7774 as certain supergiants, even if they were rank 2 based on their radial velocities, while we have removed the four stars shown spectroscopically not to be supergiants.

It is of interest to see where our supergiants fall in the various diagnostic diagrams we employed earlier. First, in Figure 5 we superimpose the actual yellow supergiants on the CMD of M31. Note that indeed our bluest "yellow" supergiants extend into the blue supergiant region, as expected, given our relaxation of our original color selection to include stars as blue as $B - V = 0$ (Section 2.1).

We next show in Figure 13 the locations of our yellow supergiants in the two-color diagram. We see that, had we relied upon a two-color plot to eliminate yellow supergiant candidates, we would have missed a number whose $U-B$ colors are more negative than would be expected from the nominal supergiant sequence (shown in red). Of course, it could be that some of the stars with $B - V > 0.4$ but $U - B < 0.1$ will turn out to be foreground upon additional spectroscopy as none of the four rank-1 stars in this region yet have confirming O I λ7774 spectroscopy. We have examined the spatial location of these four stars, however, and find that they are both in the spiral arms and near to other rank-1 yellow supergiants. We, therefore, feel that it is more likely this that is a combination of photometric errors, slightly variable reddening, and uncertainties in the two-color relation for yellow supergiants.

Finally, we show in Figure 14 the spatial distribution of our supergiant candidates in M31, where the blue symbols indicate the certain ones (either rank 1 or spectroscopically confirmed), and the red symbols the rank-2 candidates. For the most part, the yellow supergiants are found along the CO ring where star formation is most active, as expected.

4. THE H-R DIAGRAM

In Figure 15, we show the location of our 116 yellow supergiant candidates in the HRD, along with the $z = 0.040$ evolutionary tracks. For simplicity, we have shown only the newer models which include an initial rotation of 300 km^{-1} ("S3" in Table 1) as we view these as the most physically realistic. Several of these "S3" tracks were computed specifically for this project, and that of Massey et al. (2009).

First, we find that the tracks do a good job of predicting the locations of yellow supergiants in the HRD. The most luminous yellow supergiants in our sample have $\log L/L_\odot \sim 5.6$. We do *not* find yellow supergiants with luminosities of (say) $\log L/L_\odot \sim 6$, and this is in accord with what the evolutionary tracks predict. Note that with the older tracks (dotted tracks in Figure 3) we might have expected to see some higher mass, warmer yellow supergiants. Indeed, the number of high-luminosity yellow supergiants should have been similar to that seen for lower luminosity 12–20 $M_\odot$ yellow supergiants, as the older 60 $M_\odot$ track extended into the yellow supergiant realm, and the duration of the yellow supergiant phase was 5400 years (comparable to that of the lower masses as seen in Table 1).

This agreement with the new tracks is similar to what Massey et al. (2009) found for the coolest supergiants ($T_{\rm eff} \leqslant 3800$ K) in terms of the excellent agreement between the location of the tracks (and in particular the upper luminosities) and the observed locations of the stars. M31's RSGs have a maximum luminosity of $\log L/L_\odot \sim 5.4$, a little bit lower than the most luminous

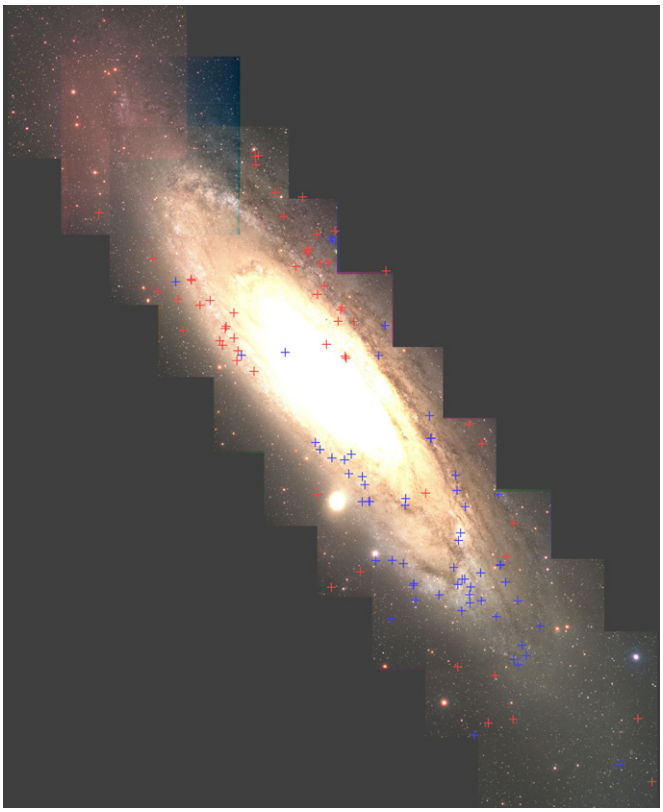

Figure 14. Distribution of our yellow supergiants across the face of M31. The blue symbols represent the rank 1 (certain) yellow supergiant candidates, while red represents the rank-2 (less certain) candidates (compare with Figure 5).

(A color version of this figure is available in the online journal.)

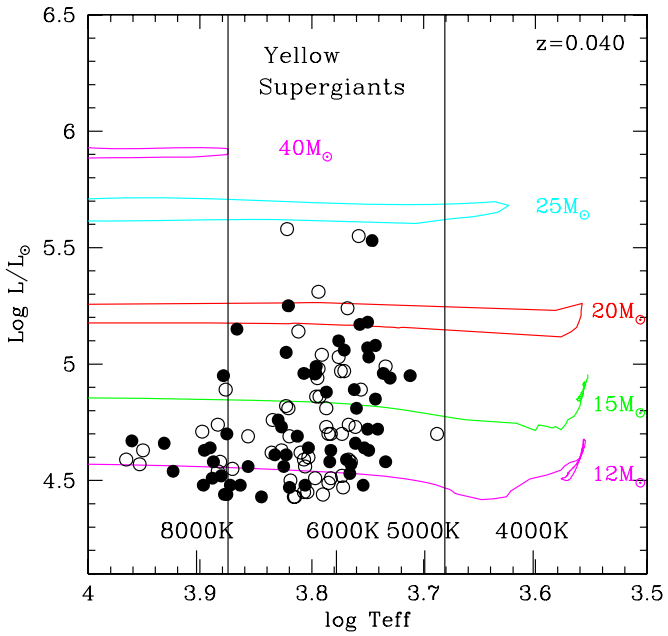

Figure 15. HRD. For simplicity, we show only the latest ($z = 0.040$) Geneva tracks with an initial rotation of 300 km s^{-1}; the location of the older tracks can be seen in Figure 3. The solid points are our certain yellow supergiants (either rank 1 or spectroscopically confirmed rank 2) while the open points are the as-yet unconfirmed rank-2 yellow supergiant candidates.

(A color version of this figure is available in the online journal.)

yellow supergiants, as might be expected from the evolutionary tracks shown in Figure 15, as the 25 $M_\odot$ track does not extend to such cool effective temperatures.

We now tackle the test we described in Section 1.1, namely to see whether the relative number of yellow supergiants increases as we go to higher luminosities as the lifetimes in Table 1 suggest to us. A visual inspection of Figure 15 shows that the answer is clearly no: the number of yellow supergiants decreases. But, let us attempt a more quantitative assessment.

We list in Table 6 the number of yellow supergiants we find in each mass bin, both for the entire sample (rank 1 and rank 2) and for just those we are most certain are actually supergiants (rank 1). We then normalize these to the number of stars in the lowest mass bin, 12–15 $M_\odot$. What we *observe* is a decreasing number of yellow supergiants as we go up in mass. At the bottom of Table 6 we have included an "extra" mass bin, 15–25 $M_\odot$, as it is clear from Table 1 that the evolutionary tracks predict a much longer lifetime for the 20 $M_\odot$ model than for either the 15 $M_\odot$ or the 25 $M_\odot$, and we wanted to see what the agreement would look like if we ignored this track.

We can estimate the number of yellow supergiants we expect from the models if we assume "steady state" star formation in M31. By this, we require only that the star formation rate *averaged over the entire disk* has stayed about the same for the past 20 Myr. In that case, the number of stars N in a particular evolutionary phase within a mass bin extending from one mass (m_1) to another (m_2) will just be

$$N_{m_1}^{m_2} = [m^\Gamma]_{m_1}^{m_2} \times \bar{\tau},$$

where Γ is the slope of the initial mass function (taken here to be -1.35 following Salpeter 1955; see also Massey 1998b), and $\bar{\tau}$ is the average duration of the evolutionary phase for masses m_1 and m_2. In the final column of Table 6 we give the expected number according to the "S3" models. We have normalized the expected numbers relative to that of 12–15 $M_\odot$.

Here we find relatively poor agreement. According to the models, the evolutionary timescale for the yellow supergiant phase increases significantly with mass (Table 1), more than compensating for the loss of stars due to the mass function. Thus we expect to find $\sim 9\times$ more yellow supergiants between the 15 and 20 $M_\odot$ tracks than those between the 12 and 15 $M_\odot$, or $\sim 6\times$ more between the 20 and 25 $M_\odot$ tracks than those between the 12 and 15 $M_\odot$ tracks. But, in reality, we find, 0.7–0.8 $\times$ and 0.2$\times$ as many, respectively. (Note that our results are insensitive to whether we count "all" of our candidates or just the certain ones.) Mostly this comes about because of the very long time predicted for the 20 $M_\odot$ yellow supergiant stage relative to that of the lower masses (78,300 years versus 5300 years). If we ignore the 20 $M_\odot$ track we find only slightly better agreement, as the number of stars observed in the 15–25 $M_\odot$ is about the same as in the 12–15 $M_\odot$ track, while the models predict 4$\times$ as many. In addition, the models predict 6$\times$ as many 25–40 $M_\odot$ yellow supergiants as those of 12–15 $M_\odot$. Based on this we expect to find 110–150 yellow supergiants with masses of 25–40 $M_\odot$, but instead we observe *none*. We can tell from Table 6 that the problem would be even worse if we had used the predictions of the "Old" $z = 0.040$ tracks, as the lifetimes are even longer for stars with masses $\geqslant$25 $M_\odot$.

We do note that the 40 $M_\odot$ just barely enters the yellow supergiant realm. The long duration of this time stage reflects the fact that the star takes some time to turn around there. We also recall that in our sample we included stars that had bluer colors than our definition of yellow supergiants. So, if there were an abundance of such stars we would expect to have observed

Table 6
Number of Yellow Supergiants Compared to Models

Mass	#	#	Ratio Relative to 12–15 $M_\odot$		
Range	All	Certain	All	Certain	Models
12–15 $M_\odot$	41	20	1.0	1.0	1.0
15–20 $M_\odot$	28	16	0.7	0.8	8.7
20–25 $M_\odot$	8	4	0.2	0.2	5.7
25–40 $M_\odot$	0	0	0.0	0.0	5.5
15–25 $M_\odot$	36	20	0.9	1.0	3.6

them, and, yet, none show up in the HRD. Nevertheless, if we were to assume that the duration of the 40 $M_\odot$ yellow supergiant phase was 0 years, rather than the 50,800 years we have included, then the number of expected stars between 25 and 40 $M_\odot$ would be 1.5× that of the 12–15 $M_\odot$ yellow supergiants. Thus rather than the 110–150 between the 25 and 40 $M_\odot$ we expect by using the 40 $M_\odot$ lifetime, we would only expect 30–60 stars between 25 and 40 $M_\odot$. However, this still results in a significant discrepancy with observations, as we observe *no* yellow supergiants in this mass range.

We emphasize that even though we expect some minimal contamination of our sample by foreground objects, the *maximum* contamination for the rank-1 objects ("mostly certain") is 15%. However, we obtain essentially the same ratios in Table 6 whether we count all of our candidates (rank 1 and rank 2) or just the rank-1 stars. So, it appears that our conclusion is robust.

Recall also from Figure 5 that if anything our radial velocity survey was slightly biased toward the brighter stars than the fainter. We have made no allowance for this in the observed ratios in Table 6, but to do so would *increase* the discrepancy. The typical 12–15 $M_\odot$ stars have $M_V = -7$, or $V = 17.8$, while the 20–25 $M_\odot$ stars have $M_V = -9$, or $V = 15.8$. The lower mass stars are therefore under represented by perhaps a factor of $\sim$ 1.5. Thus the 0.2 nominal observed ratio of the 20–25 $M_\odot$ stars relative to the 12–15 $M_\odot$ stars should actually be lower by a factor of 1.5, suggesting that the disagreement with the 5.6 ratio predicted by the models is about a factor of 40.

Is this a problem with the higher mass evolutionary tracks predicting too long a timescale for the yellow supergiant stage, or with the lower mass tracks predicting too short a timescale? We can answer this indirectly by computing their expected lifetimes based upon the relative number of yellow supergiants and unevolved (O-type) stars observed. Using the LGGS data, Massey (2009) estimates the number of unevolved massive stars with masses > 20 $M_\odot$ is about 24,800 in M31. The IMF-weighted H-burning lifetime is of order 5 Myr, and, assuming a constant star formation rate, we would thus expect to see 5×10^{-3} massive stars born each year. We observe eight total (certain and probable) yellow supergiants above 20 $M_\odot$. Recall that our sample contains only 68% of the stars located in the region for which we expect radial velocities to be < -150 km s^{-1}, and that region covered 73% of the area of the entire LGGS, from which the number of unevolved massive stars was estimated. We expect then that the true number of yellow supergiants with masses$>$ 20 $M_\odot$ is about 16. Therefore, we can estimate the actual ages of the yellow supergiant stage as $16/24800 \times 5$ Myr. This is about 3200 years, which is consistent with the life times the 12–15 $M_\odot$ models predict, but is at variance with the much longer timescales predicted by the models for higher mass yellow supergiants. We suggest that these are too long by more than an order of magnitude.

Could this discrepancy instead be an argument that the global star formation rate in M31 has in fact not been constant over the past 20 Myr? Yellow supergiants of 12 $M_\odot$ are roughly 17 Myr old, according to the models, while those of 25 $M_\odot$ are only 7 Myr. So, if during that 10 Myr period the overall star formation rate had decreased by a factor of 30–40 that would roughly compensate for the smaller number of stars that we find. However, such a drastic change is in conflict with other observations. Williams (2003) analyzed the LGGS photometry and concluded that there has been a slight (25%) increase in the star formation rate since 25 Myr ago. This is a marginal result, and consistent with constant star formation to within 2σ (see his Table 2), but it certainly precludes the possibility of a 3000%–4000% decrease over a similar time span.

5. SUMMARY, DISCUSSION, AND FUTURE WORK

We measured radial velocities for $\sim$ 2900 stars in M31, identifying 54 as rank 1 (nearly certain supergiants) and 66 as rank 2 (probable supergiants). Follow-up spectroscopy eliminated four of the rank-2 stars, while confirming others as supergiants. The magnitude limits we chose should make our sample complete down to 12 $M_\odot$. In all we observed 68% of the target candidates and the sample was restricted to the 73% of the LGGS area that should have radial velocities < -150 km s^{-1}. So, the true number of yellow supergiants should be about a factor of 2.0 larger than what we find. The foreground contamination is proved to be 96%–98%. There may be a few halo yellow giants among our candidates, but comparison with the Besancon model suggests this should be minor, at most 15% for the rank-1 objects based purely upon the distribution of radial velocities. In practice, we expect this contamination to be considerably less, since we replied upon the difference between the observed and expected velocities (where the latter is dependent upon position in the galaxy) to assign rank and membership. Nevertheless, it would be very useful to conduct follow-up spectroscopy of the rank-2 objects in order to ascertain which have strong O I λ7774 absorption or other spectral indicators of high luminosity.

We compared the location and numbers of yellow supergiants in the HRD to those expected from the Geneva evolutionary tracks. We find excellent agreement between the locations of stars in the HRD and the tracks: there are not (for instance) high-luminosity yellow supergiants with moderate temperatures that are inconsistent with the tracks. Rather, the inconsistencies we do note are related to the lifetimes predicted by the models for the yellow supergiant stage. The number of yellow supergiants decreases with increasing luminosity (mass), with no stars found more massive 25 $M_\odot$. Yet, the long duration of the yellow supergiant phase predicted by the models for 20–40 $M_\odot$ suggests that we should see far more high-luminosity yellow supergiants than what we observe. Comparing the number of yellow supergiants we find to the number of unevolved O-type

stars, suggests that the typical duration of the yellow supergiant stage for stars with masses $> 20\ M_{\odot}$ should be 3000 years, similar to what the models predict for 12–15 $M_{\odot}$ Yet, the models predict lifetimes far greater than this.

We do not yet have an adequate explanation for the discrepancy, but will address this in future work. The higher mass tracks (for which the predicted yellow supergiant lifetimes appear to be too long) show the stars evolving back to the blue after the RSG stage. If instead the stars ended their lives as RSGs, without this loop back to the blue, then the predicted yellow supergiant phase would be shorter as the star would pass through this region only once. This might be the case if the mass loss during the RSG stage had been significantly over-estimated. In part, this could be tested by comparing the number of observed WRs with that of RSGs. The number of WRs in M31 is not known well enough to make this comparison as yet. Alternatively, it could be that the blue loops are present, but that the mass-loss rates during the evolution bluewards have been underestimated. A sensitive test would be to conduct abundance studies of the yellow supergiants in this region of the HRD to look for evidence that any of these stars are in a post-RSG phase. An additional test would be to look for circumstellar material left from the slow dense wind of the RSG stage around any of these objects.

It would, of course, be of interest to extend this work to galaxies with other metallicities, such as the Magellanic Clouds, where the unevolved massive star content is also known, and where the models predict long lifetimes for yellow supergiants even for 12–15 $M_{\odot}$ stars (Table 1). We hope to carry out such work ourselves during the next observing season.

We gratefully acknowledge the fine support at the MMT Observatory. M.R.D.'s work was supported through a National Science Foundation REU grant, AST-0453611, while P.M.'s efforts were supported through AST-0604569. We are grateful to the Kitt Peak National Observatory Director, Buell Jannuzi, and to Di Harmer for their efforts in obtaining the follow-up spectra; Harmer and Brian Skiff also offered useful advice that aided in our interpretation of these data. Knut Olsen made useful comments on the recent star formation history of M31, and Heather Morrison provided useful correspondence on the issue of foreground halo stars. We also thank the anonymous referee for useful suggestions that improved the paper.

REFERENCES

Bahcall, J. N., & Soneira, R. M. 1980, ApJS, 44, 73
Bertin, E., & Arnouts, S. 1996, A&AS, 117, 393
Binney, J., & Merrifield, M. 1998, Galactic Astronomy (Princeton, NJ: Princeton Univ. Press), 673
Caldwell, N., Harding, P., Morrison, H., Rose, J. A., Schiavon, R., & Kriessler, J. 2009, AJ, 137, 94
Charbonnel, C., Meynet, G., Maeder, A., Schaller, G., & Schaerer, D. 1993, A&AS, 101, 415
Courteau, S., & van den Bergh, S. 1999, AJ, 118, 337
Crockett, N. R., Garnett, D. R., Massey, P., & Jacoby, G. 2006, AJ, 131, 2478
Fabricant, D., et al. 2005, PASP, 117, 1411
FitzGerald, M. P. 1970, A&A, 4, 234
Flower, P. J. 1996, ApJ, 469, 355
Freedman, W. L. 1988, AJ, 96, 1248
Galleti, S., Bellazzini, M., Federici, L., Buzzoni, A., & Fusi Pecci, F. 2007, A&A, 471, 127
Gilbert, K. M., et al. 2006, ApJ, 652, 1188
Hartmann, D., & Burton, W. B. 1997, Atlas of Galactic Neutral Hydrogen (Cambridge: Cambridge Univ. Press)
Hodge, P. W. 1981, Atlas of the Andromeda Galaxy (Seattle: Univ. Washington Press)
Humphreys, R. M. 1978, ApJS, 38, 309
Humphreys, R. M. 1979, ApJ, 234, 854
Humphreys, R. M., Massey, P., & Freedman, W. L. 1990, AJ, 99, 84
Humphreys, R. M., Pennington, R. L., Jones, T. J., & Ghigo, F. D. 1988, AJ, 96, 1884
Hurley-Keller, D., Morrison, H. L., Harding, P., & Jacoby, G. H. 2004, ApJ, 616, 804
Keenan, P. C., & McNeil, R. C. 1976, An Atlas of Spectra of the Cooler Stars (Columbus: Ohio State Univ. Press)
Kippenhahn, R., & Weigert, A. 1990, Stellar Structure and Evolution (Berlin: Springer), 468
Koch, A., et al. 2008, ApJ, 689, 958
Kovtyukh, V. V. 2007, MNRAS, 378, 617
Kurucz, R. L. 1992, in The Stellar Populations of Galaxies, ed. B. Barbury & A. Renzini (Dordrecht: Kluwer), 225
Maeder, A., & Meynet, G. 2000, ARA&A, 38, 143
Maeder, A., & Meynet, G. 2001, A&A, 373, 555
Magnier, E. A., Lewin, W. H. G., van Paradijs, J., Hasinger, G., Jain, A., Pietsch, W., & Trumper, J. 1992, A&AS, 96, 379
Massey, P. 1998a, ApJ, 501, 153
Massey, P. 1998b, in ASP Conf. Ser. 142, The Stellar Initial Mass Function, 38th Herstmonceux Conference, ed. G. Gilmore & D. Howell (San Francisco, CA: ASP), 17
Massey, P. 2009, in Hot and Cool: Bridging Gaps in Massive Star Evolution, ed. C. Leitherer et al. (San Francisco, CA: ASP), arXiv:0903.0155
Massey, P., Armandroff, T. E., & Conti, P. S. 1986, AJ, 92, 1303
Massey, P., Lang, C. C., DeGioia-Eastwood, K., & Garmany, C. D. 1995, ApJ, 483, 188
Massey, P. 2003, ARA&A, 41, 15
Massey, P., McNeill, R. T., Olsen, K. A. G., Hodge, P. W., Blaha, C., Jacoby, G. H., Smith, R. C., & Strong, S. B. 2007a, AJ, 134, 2474
Massey, P., Olsen, K. A. G., Hodge, P. W., Jacoby, G. H., McNeill, R. T., Smith, R. C., & Strong, S. B. 2007b, AJ, 133, 2393
Massey, P., Olsen, K. A. G., Hodge, P. W., Strong, S. B., Jacoby, G. H., Schlingman, W., & Smith, R. C. 2006, AJ, 131, 2478
Massey, P., Silva, D. R., Levesque, E. M., Plez, B., Olsen, K. A. G., Clayton, G. C., Meynet, G., & Maeder, A. 2009, ApJ, 703, 420
Meynet, G., & Maeder, A. 2003, A&A, 404, 975
Meynet, G., & Maeder, A. 2005, A&A, 429, 581
Mink, D. J., & Kurtz, M. J. 2001, in ASP Conf. Ser. 238, Astronomical Data Analysis Software and Systems X, ed. F. R. Harnden, Jr., F. A. Primini, & H. E. Payne (San Francisco, CA: ASP), 491
Mink, D. J., Wyatt, W. F., Caldwell, N., Conroy, M. A., Furesz, G., & Tokarz, S. P. 2007, in ASP Conf. Ser. 376, Astronomical Data Analysis Software and Systems XVI, ed. R. A. Shaw, F. Hill, & D. J. Bell (San Francisco, CA: ASP), 249
Morrison, H. 1993, AJ, 106, 578
Oestreicher, M. O., & Schmidt-Kaler, Th. 1999, Astron. Nachr., 320, 105
Osmer, P. S. 1972, ApJS, 24, 247
Przybilla, N., Butler, K., Becker, S. R., Kudritzki, R. P., & Venn, K. A. 2000, A&A, 359, 1085
Robin, A. C., Reylé, S., & Derrière, Picaud S. 2003, A&A, 409, 523
Rubin, V. C., & Ford, W. K., Jr. 1970, ApJ, 159, 379
Salpeter, E. E. 1955, ApJ, 121, 161
Schaerer, D., Charbonnel, C., Meynet, G., Maeder, A., & Schaller, G. 1993, A&AS, 102, 339
Schaller, G., Schaerer, D., Meynet, G., & Maeder, A. 1992, A&AS, 96, 269
Sofue, Y., & Kato, T. 1981, PASJ, 33, 449
Tonry, J., & Davis, M. 1979, AJ, 84, 1511
van den Bergh, S. 2000, The Galaxies of the Local Group (Cambridge: Cambridge Univ. Press)
Williams, B. F. 2003, AJ, 126, 1312
Zaritsky, D., Kennicutt, R. C., & Huchra, J. P. 1994, ApJ, 420, 87